Zeinab Mousavi Karimi

MODELLING, IMPLEMENTATION AND PERFORMANCE ANALYSIS OF A HYBRID WIND-SOLAR POWER GENERATOR WITH BATTERY STORAGE

Fevereiro 2014

· U C ·

UNIVERSIDADE DE COIMBRA

Acknowledgement

The success of any project depends largely on the encouragement and guidelines of many others aside from the author's efforts and hard work. I take this opportunity to express my gratitude to the people who have been instrumental in the successful completion of this Master of Science thesis. I would like to show my greatest appreciation to my supervisor, Professor Sérgio Cruz. I cannot thank him enough for his tremendous support and help. I felt motivated every time I attended his meetings and without his encouragement and guidance this project would not have materialized.

I would also like to thank my husband, Mohammad, and my parents for the endless love, support and faith they have given me during the past one year it has taken me to finalize this thesis.

The guidance and support received from all the members who contributed to this work, was vital for its success. I am grateful for their constant help and support.

Finally, his work has been framed under the Initiative Energy for Sustainability of the University of Coimbra and supported by the Energy and Mobility for Sustainable Regions Project CENTRO-07-0224-FEDER-002004.

Abstract

A wind-solar hybrid power generator system consisting of photovoltaic (PV) modules controlled by maximum power point tracking (MPPT) method and connected to a DC-DC boost converter, a grid-connected wind turbine coupled with a permanent magnet synchronous generator (PMSG) and connected to a back-to-back converter and also a bidirectional DC-DC converter, and finally an energy storage module (batteries) connected to a bidirectional DC-DC converter has been modelled, implemented and discussed in this thesis to achieve an efficient and cost-effective system configuration so that renewable energy power sources could improve the life of people in both urban and remote residential areas. The entire model is implemented in the MATLAB/Simulink environment. The behaviour of the proposed model is examined and the output voltage and power characteristics of the model obtained from simulations are analysed and optimized using the proposed control strategy. The model is further analysed from an economic point of view so that consumers planning to install the system can get an idea of the system costs.

Keywords: MATLAB, Simulink, PV, wind turbine, battery, simulation, controller, DC-DC boost converter, back-to-back converter, bidirectional converter, MPPT, grid-connected

Table of Contents

List of Figures

List of Tables

List of Symbols

N_{cycles}	Number of cycles for which the battery can release its energy	
R_{sh}	Parallel resistance in a PV cell model	Ω
R_s	Series resistance in a PV cell model	Ω
I_{ph}	Photocurrent	A
I_d	Diode's reverse saturation current	A
q	Electric charge	C
v_d	Voltage across the diode	V
K	Boltzmann's constant	J/K
T_c	PV cell absolute temperature	K
N	Ideality factor of the diode	
K_i	PV cell's short circuit current temperature coefficient	A/°C
G	Variable solar radiation	W/m^2
I_{PV}	PV cell's short-circuit current	A
V_{PV}	PV cell's open-circuit voltage	V
P_{PV}	Power produced by PV cell	W
$\eta_{converter}$	Power conversion efficiency	
v_L	Inductor voltage	V
V_g	DC source voltage in DC-DC boost converter circuit	V
i_c	Capacitor current	A
D	Duty cycle	
$M(D)$	Voltage conversion ratio	
V_{DC}	DC voltage	V
P_m	Mechanical output power of wind turbine	W
c_p	Performance coefficient of wind turbine	
ρ	Air density	kg/m^3
A	Wind turbine swept area	m^2
v_{wind}	Wind speed	m/s
λ	Tip speed ratio	
β	Blade pitch angle	Degrees
T_w	Wind turbine rotor torque	Nm
ω_m	Wind turbine rotor angular velocity	Rad/s
R	Rotor radius	m
P_{m_pu}	Power in per unit of the nominal power	
k_p	Power gain	
n	Gear ratio	
θ	Angle between the turbine rotor and the generator rotor	Rad
ω_r	Generator rotor speed	Rad/s
T_e	Electromagnetic torque	Nm
L_{sq}	q-axis inductance	H
L_{sd}	d-axis inductance	H

i_{sq}	q-axis current	A
i_{sd}	d-axis current	A
v_{sq}	q-axis voltage	V
v_{sd}	d-axis voltage	V
p	Number of pole pairs	
B	Friction factor	Nms
V_{ref}	Reference voltage	V
$P_{peak\ panels}$	Peak power produced by solar panels	W
$P_{peak,usage}$	Peak power used	W
$E_{produced}$	Energy produced by the PV system	kWh
E_{used}	Amount of energy used by the PV system	kWh
T_{sun}	Average number of hours of sunlight per day of month	Hours
$Cost_{panels}$	Cost of the solar panels	€
$Cost_{WT}$	Cost of a wind turbine	€
$Cost_{inverter}$	Costs of inverter	€
E_{stored}	Number of kWh which can be stored by batteries	kWh
$Cost_{upfront}$	Total cost of wind-solar hybrid power system	€
V_{nom}	Battery's nominal voltage	V
Q_{rated}	Battery's rated capacity	Ah
V_{full}	Battery's fully-charged voltage	V

List of Abbreviations

Abbreviation	Description
Ah	Ampere-hour
BESS	Battery Energy Storage System
CHP	Combined Heat and Power
DOD	Depth of Discharge
EDP	Energias de Portugal
FET	Field Effect Transistor
GHG	Greenhouse Gas
GTO	Gate Turn-Off Thyristor
IGBT	Integrated-Gate Bipolar Transistor
KCL	Kirchhoff's Current Law
KVL	Kirchhoff's Voltage Law
kWh	Kilowatt-hour
MOSFET	Metal-Oxide Semiconductor Field-Effect Transistor
MPPT	Maximum Power Point Tracking
PHSS	Pumped Hydroelectric Storage System
PMSG	Permanent Magnet Synchronous Generator
PMSM	Permanent Magnet Synchronous Machine
PSF	Power Signal Feedback
PV	Photovoltaic
PWM	Pulse Width Modulation
RES	Renewable Energy System
SMESS	Superconducting Magnetic Energy Storage System
SOC	State Of Charge

Outline

This Master of Science thesis includes six chapters. Chapter 1 gives a general introduction to the work, discusses the motivation behind the thesis, and outlines the thesis description. Chapter 2 begins with a literature review on the existing wind-solar hybrid power system topologies and concludes with the selected topology. Chapter 3 discusses the theory of the elements used in residential renewable energy power generator systems. Chapter 4 explains the procedures and the steps required to model and implement the wind-solar hybrid generator in Simulink using the necessary equations and figures. Chapter 5 hosts a performance analysis on the final wind-solar hybrid system and discusses the system from an economic point of view. Chapter 6 presents final conclusions of this thesis and offers recommendations for future work.

1. Introduction

One of the most promising applications of renewable energy technology is the installation of wind-solar hybrid power generator systems in urban and remote areas in developing and under-developed countries, where globally over 1.3 billion people are reported to live without access to electricity. In order for remote areas to be electrified, they can either extend the grids of the existing power systems or they can build new isolated power systems, which are alternative sources of energy. In general, it is more favourable to go for the former method, despite the fact that they are not always affordable and demand large investment for grid extension [1].

Figure 1.1 below shows the cost effectiveness of wind-solar power systems, when compared to the conventional energy sources, over their lifetime in India and Tanzania for village electrification. The initial cost of such (renewable) systems is higher than the conventional source. However, the large fuel cost, transportation costs, replacement and maintenance costs of the conventional source throughout its life overshadow its lower initial cost [2].

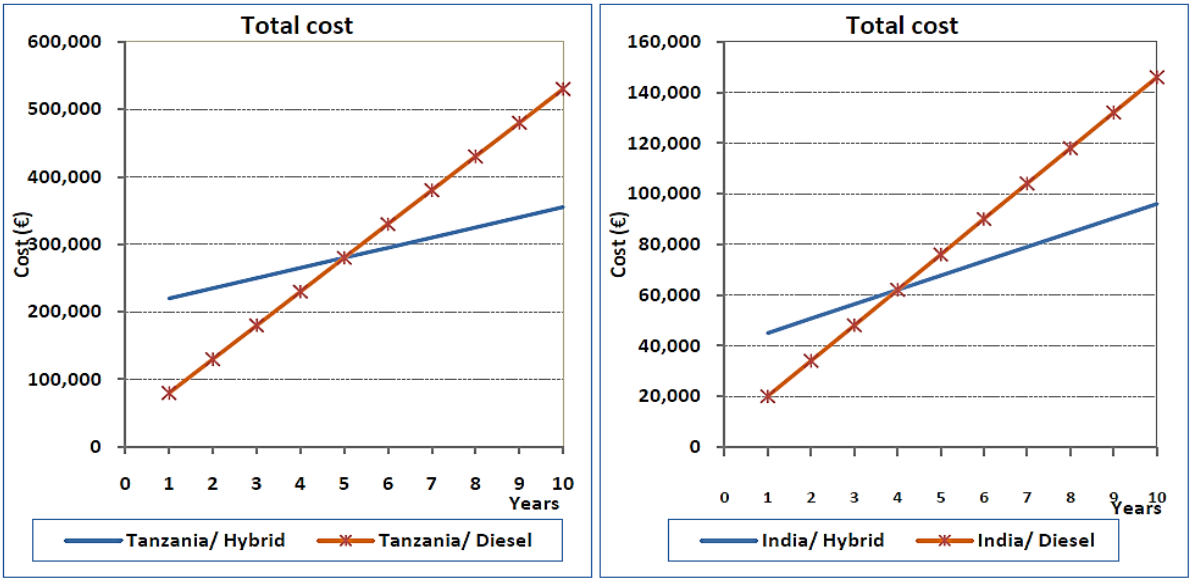

Figure 1.1 Economical comparison: diesel versus wind-solar hybrid power system [2].

So, although the initial investment for wind-solar power systems is high, the low running cost and overall lifetime cost attracts users over conventional energy sources. Recent research and development of alternative energy sources have shown excellent potential for utilizing renewable

energy sources, for example solar energy, wind energy, or a combination of both to provide a reliable power supply to residential (urban and remote) areas. Wind and solar energy have been particularly popular ones owing to their abundance in nature, ease of availability and convertibility to electric energy in a sustainable way to supply the necessary power demand and thus to elevate the living standards of the people with/without access to the electricity grid [3].

1.1 Incentives

While having numerous benefits in producing power, over the past few years, hybrid technology has been developed and upgraded its role in renewable energy sources. Nowadays many houses in urban and rural areas use hybrid systems. Many isolated islands also try to adopt this kind of technology because of the benefits which can be received in comparison with a single renewable system [1].

The wind-solar hybrid system presents many benefits: it can be operated during the day using the energy from the sun and after the sun has set, it can utilise the potential wind energy to continue its function. For this reason, wind and solar systems work well together in a hybrid system and they provide a more consistent year-round output than stand-alone PV or wind systems. Moreover, with the use of the appropriate auxiliary systems like batteries it is possible to store energy which will be useful in compensating electrical demands used by the building for periods when there is no sun or wind. Finally, it is economically advantageous to use non-finite, sustainable resources. The investment in modern technologies both environmentally and economically will win through the generations to come in the fight for energy efficiency and effectiveness [4].

As well as a grid-connected system – which is the focus of this thesis – a grid-independent wind-solar hybrid power generator system can be highly beneficial too. There are many remote places, especially in under-developed and developing countries, where grid supply has not reached yet but with the availability of solar-wind hybrid systems, they have the chance to gain access to electricity as well [5]. Over and above, the dependence of humans on depleting fossil fuels and the adverse environmental effects of conventional power generation systems created renewed interest in renewable energy sources toward building a sustainable energy economy.

Furthermore, a hybrid power system has the ability to provide 24/7 electricity to the load. This system offers a high efficiency, flexibility and environmental benefits. The system also gives the opportunity for expanding its capacity in order to cope with the increasing demand in the future. This can be done by increasing the rated power of the renewable generator [3].

Finally, the disadvantage of standalone (non-hybrid) power systems is that the availability of renewable energy sources has daily and seasonal patterns which results in difficulties of regulating the output power to cope with the load demand and also, a very high initial investment cost is required. Combining the renewable energy generation systems together such as a hybrid wind-solar power generator system will enable the power generated from renewable energy sources to be more reliable, affordable and used more efficiently.

1.2 Thesis Description

The combination of different renewable energy sources, such as a wind turbine and a PV system is known as a hybrid power system. As mentioned earlier, wind-solar hybrid systems can provide a steady community-level electricity service including residential electrification.

This thesis focuses on the combination of wind, solar, and energy storing systems for sustainable power generation. The wind turbine output power varies with different wind speeds and the solar energy also varies with the hourly, daily and seasonal variation of solar irradiation. Thus, a proper controller-converter system as well as a battery module (energy storage bank) can be integrated with the wind turbine and the PV system to ensure that the system performs under all conditions.

In the proposed system, when the wind speed is sufficient, the wind turbine can meet part of the AC load demand. When there is enough energy from the sun, a portion of the DC load demand can be supplied from the wind turbine and the PV-array system. Whenever there is an excess supply from the system, the energy storage bank stores energy from the wind turbine and the PV arrays which will be fed to DC loads at times when there are insufficient supplies from the wind-solar system. Also, at times when there are insufficient winds and the PV system has more energy required for the DC load and also the battery is fully charged, the PV system has the ability to send its energy to the grid.

Figure 1.2 shows a schematic description of the wind-solar hybrid system used in this thesis, where the energy produced from the different sources reaches the consumption areas after power electronic devices are integrated with the PV and the wind turbine module to convert one form of power into another, control the overall power flow and enhance the efficiency of the whole system.

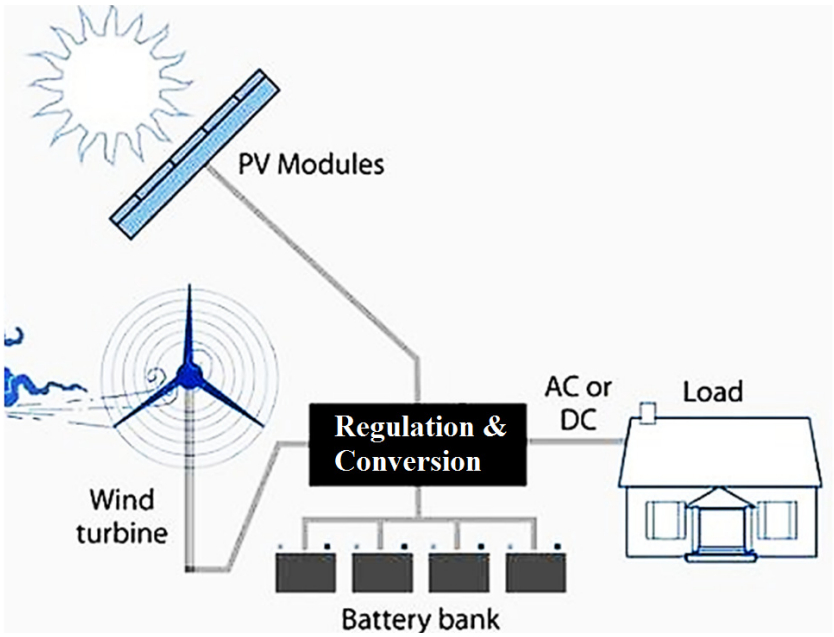

Figure 1.2 Schematic of the proposed wind-solar hybrid power system.

The proposed hybrid system was designed for a small 2-bedroom building in a residential area of Lisbon, Portugal. With the use of specific hybrid topologies the extent to which these systems can span the energy demands of the building was investigated. Then, a cost analysis was performed for the final arrangement of the complete wind-solar power generator system so that the economic feasibility and the financial payoff period could be estimated.

2. Literature Review

Over the past few years several researches have been carried out on hybrid power systems, such as Yang [6], who recommended an optimal design model for the wind-solar hybrid power system, which employs battery banks to calculate the system optimum configurations in China. Dihrab [7] presented a hybrid solar-wind system as a renewable source of power generation for grid-connected application in three cities in Iraq. The proposed system was simulated using MATLAB, in which the input parameters for the software were the meteorological data for the selected locations and the sizes of PV and wind turbines. Dihrab's results showed that it is possible for Iraq to use the solar and wind energy to generate enough power for some villages in the desert or rural area.

Reichling [8] modelled a hybrid solar-wind power plant in south western Minnesota for a two year period, using hourly solar irradiation and wind speed data. Reichling compared the market value of energy produced, retail value of energy produced, and the levelized cost of energy of the hybrid plant to those of an energy equivalent wind-only plant. The results showed that adding solar thermal electric generating capacity to a wind farm rather than expanding with additional wind capacity provides cost–benefit trade-offs. Ekren [9], showed an optimum sizing procedure of wind-PV hybrid system in Turkey.

Several modelling studies on PV-wind turbine power system have been conducted. Among them, Kim [10] developed a grid-connected photovoltaic model using PSCAD for electromagnetic transient analysis where a simple circuit model of the solar array was used to easily simulate its inherent characteristics with the basic specification data. Tsai [11] implemented an insulation-oriented PV model using the MATLAB/Simulink software package. Taking the effect of sunlight irradiance on the cell temperature, the model took ambient temperature as reference input and used the solar insolation as a unique varying parameter. The output current and power characteristics were simulated and analysed using the proposed PV model. The model verification was finally confirmed through an experimental measurement.

Gow [12] developed a general PV model which could be implemented on simulation platforms such as PSPICE. The model accepted irradiance and temperature as variable parameters and

outputted the V-I characteristic for the particular cell used in the paper under certain conditions. Khan [13] presented the model of a small wind-fuel cell hybrid energy system and analysed the life cycle of a wind-fuel cell integrated system. Dynamic aspects of temperature variation and double layer capacitance of the fuel cell were also included in the author's paper. PID controllers were used to control the fuel cell system. Simulink was used for the simulation of this nonlinear hybrid energy system. System dynamics were studied to determine the voltage variation throughout the system and an analysis of the simulation results and limitations of the wind–fuel cell hybrid energy system were discussed.

Hossain [14] presented a paper on modelling a wind-solar hybrid system for rural applications. The model was developed to simulate a stand-alone power system with battery storage. The model was applied to a typical consumer peak load of 1 kW at a remote community in Bangladesh. An economic analysis was also undertaken to assess the feasibility of such a system at the location considered.

Chang [15] discussed the modelling and application of a wind-solar energy hybrid power generation system based on "multi-agent" technology. Through the collaboration of multi-agents, the control system of the wind-solar topology was optimised and its intelligence and reliability were enhanced.

Castle [16] published a paper about analysing the merits of a hybrid wind-solar concept for stand-alone systems. The methods for evaluating the benefits of such systems for stand-alone applications were developed. It was discovered that the optimum mix of wind and PV power with an electrochemical storage system, with or without fossil fuel generator backup, depends upon the individual subsystem economics. A computer code was developed to calculate the optimum subsystem-sizes that could minimise the energy cost. It was found that the actual merits of a hybrid system over a pure PV or wind system depend upon many factors including load profile, wind regime, insulation, cost and availability of backup power, and so on.

CADDET Centre for Renewable Energy [17] gave a project on a wind-solar hybrid system in Bullerö Island, Sweden. This report gave ideas about how the wind-solar power installation can meet almost all the island's energy demand with less than half the cost of installing grid

connection. Thus, they proved that this method was a cost-effective use of renewable energy in remote places.

Nwosu [18] presented a paper about the balance between power and energy in wind-solar hybrid power systems. In this paper, the power and energy balance in a hybrid wind-solar system consisting of batteries and a combined heat and power (CHP) subunit was presented. A case study for winter and summer seasons were conducted in an urban city in the Netherlands. It was observed that within the period investigated, there existed an instant when the generated energy from the wind-solar hybrid system was below the energy demand of the load. The battery unit supplied this deficient energy for the system so as to maintain a steady power regime.

To allow the PV system to produce the maximum possible power, many maximum power tracking techniques and algorithms have been developed. Femia [19] and Tariq [20] suggested the most widely used method known as the Perturbation and Observation method. In their paper, a microcontroller-based maximum power point tracking (MPPT) was realized. Two tracking algorithms, namely, Perturbation and Observation algorithm and maximum power point voltage (MPPV) algorithm were implemented. The MPPT was tested under varying insolation and load conditions. It was shown that with the Perturbation and Observation algorithm, the controller took a relatively moderate time to track the maximum power point.

Other strategies used to achieve the maximum power from PV systems include the Incremental Conductance method which was proposed and implemented by Esram and Chapman [21], and also the Fractional Open Circuit Voltage method which was discussed in detail by Menniti [22], Xuesong [23], and Dorofte [24].

Mittal [25] modelled and simulated a system which included a wind turbine (WT), a PMSG, a three-phase diode rectifier bridge, a DC bus with a capacitor and a current-regulated pulse width modulation (PWM) voltage source inverter. The complete modeling of a wind power generation system with PMSG and power electronic converter interface along with the control scheme was developed using MATLAB/Simulink. The performance of the developed model was studied for different wind speeds and load conditions and the simulation results showed that the controllers were able to regulate the DC link voltage, and the active and reactive power produced by the wind power generation system.

Upadhyay [26] used a PMSG-based wind turbine system and explained that when compared with induction generators, the PMSG has a smaller physical size and a lower moment of inertia which means a higher reliability and power density per volume ratio. According to Upadhyay, the electrical losses in the rotor are eliminated on the expense of high costs for permanent magnet materials and fixed excitation, which cannot be changed according to the operating point. The model used in their study was developed in the d-q synchronous rotating reference frame.

The DC-DC power electronic interfaces of batteries used in microgrid was proposed and studied by Sofla [27]. The study was conducted to investigate how the stability of the islanded microgrid depends on its response speed to the transients. The paper focused on inner and power controllers of the DC-DC bidirectional converters for interfacing batteries in microgrid. The inner control techniques were discussed and a control strategy for the operation of batteries in different modes was proposed. Wei [28] proposed a parallel structure of bidirectional buck/boost converters and a power-tracking control scheme for wind energy storage system applications. The converter performance was studied and compared to single-unit topologies. The proposed converter was found to have smooth currents and fast dynamics which allowed a reduction in the converter switching frequency and DC filtering capacitor.

Ramprabhakar [29] gave a paper which described a control approach applied to dual bi-directional voltage source converter for composite wind-solar-hydro power systems in order for these systems to operate in grid-connected and islanded modes. A control technique was devised based on sum-of-product of load and utility voltages, which generated requisite phase angle for utility synchronization. The effectiveness of the control technique was demonstrated through simulation of the proposed scheme under constant as well as changing meteorological and load conditions.

In this thesis, a detailed model, control and simulation of a wind-solar hybrid power generation system with battery storage is proposed and implemented. Modelling and simulation are carried out using the MATLAB/Simulink software package, specifically SimPowerSystems, to verify the effectiveness of the proposed system. SimPowerSystems enables engineers to use model-based designs to model and simulate electrical circuits and power systems within Simulink, and includes a comprehensive applications library which makes the interfacing of all the components of the wind-solar-battery system a straightforward process for the user.

3. Hybrid Energy Systems for Residential Use

3.1 Introduction

Renewable energy systems (RESs) are one of the most suitable and environmentally friendly solutions to provide electricity within urban and rural areas. On-grid and off-grid electrification based on the generation of power through the installation of renewable energy power systems in urban and rural households have been proven to be capable of delivering high quality and reliable electricity for heating, lighting, and demands alike. Using RESs have many advantages over conventional sources including the following [2]:

- High accessibility to reliable electricity at any time
- Reduce the dependency on fossil fuels and from oil price fluctuations
- Increase economic productivity and create local employment opportunities
- Fight climate change
- Allow for a better use of local natural resources

Wind-solar hybrid systems can provide a steady community-level electricity service, such as residential electrification, also offering the possibility to rural areas to be upgraded through grid connection in the future. Furthermore, in case of installation and use in rural areas, due to their high levels of efficiency, reliability and long term performance, these systems can also be used as an effective backup solution to the public grid in case of natural disasters, emergencies, sudden blackouts or weak grids.

The main disadvantage of wind turbines and PV-systems is that naturally variable wind speed and variable solar irradiation cause voltage and power fluctuation problems at the load side. These problems can be solved by using appropriate power converters and proper controllers both for the PV and the wind turbine system. Another significant point is to store the energy generated by wind turbines and PV-systems for future use when no wind and/or no irradiation is available but the user demand exists. For this, an energy storage bank can be incorporated in such a way that the battery stores energy whenever there is excess supply and discharges when there is more demand than supply.

In the following sections of this chapter, the wind-solar hybrid system components are discussed one by one.

3.2 System Components

The system topology which this thesis is dealing with was designed, implemented and simulated in Chapter 4. The hybrid power system, described here, basically includes the following main elements:

1. Renewable energy sources: PV-array and wind turbine generator
2. DC-DC converters, controllers and an inverter
3. Energy storage system: Battery bank
4. AC and DC loads

The following sections give the basic descriptions for the main elements used in the various topologies discussed in Chapter 4.

3.3 PV Module

3.3.1 Introduction

With no pollutant or greenhouse gas (GHG) emission, PV cells convert sunlight directly to electricity. They are basically made up of a PN junction. Figure 3.1 shows the photocurrent generation principle of PV cells. Basically, when sunlight hits the cell, the photons are absorbed by the semiconductor atoms, freeing electrons from the negative layer. This free electron finds its path through an external circuit toward the positive layer resulting in an electric current from the positive layer to the negative one.

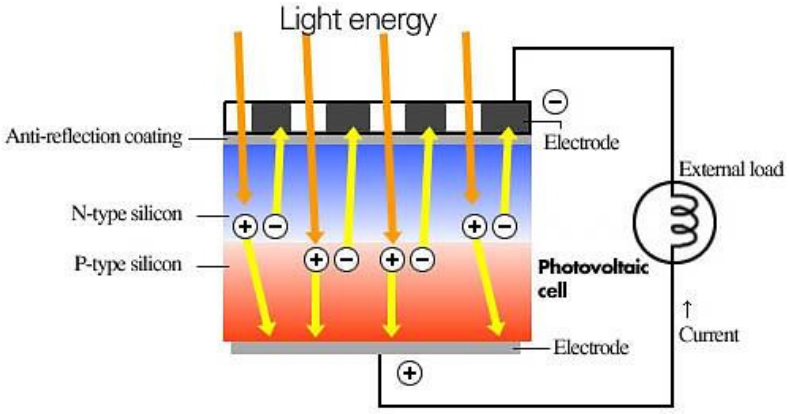

Figure 3.1 A photovoltaic cell generates electricity when irradiated by sunlight[1].

Typically, a PV cell generates a voltage around 0.4 V to 0.8 V depending on the semiconductor and the built-up technology [30]. This voltage is low enough as it cannot be of use. Therefore, to get benefit from this technology, tens of PV cells are connected in series to form a PV module. These modules can be interconnected in series and/or parallel to form a PV panel as shown in Figure 3.2. In case these modules are connected in series, their voltages are added with the same current. On the other hand, when they are connected in parallel, their currents are added while the voltage is the same.

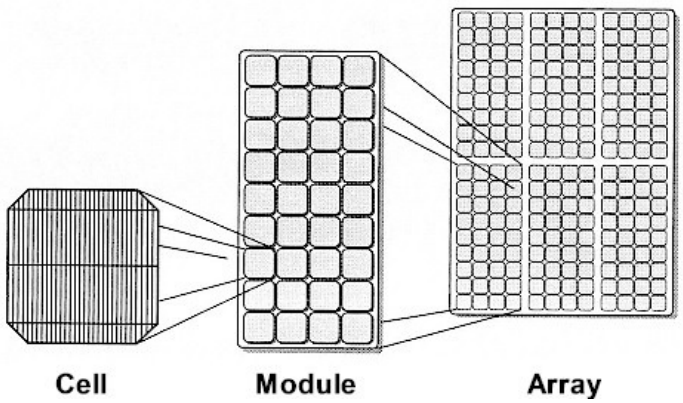

Figure 3.2 Building blocks of solar electricity[2].

Three major families of PV cells include monocrystalline technology, polycrystalline technology and thin film technologies. The monocrystalline and polycrystalline technologies are based on microelectronic manufacturing technology and their efficiency generally between 10% and 15%

[1] Image obtained online from: http://www.apec-vc.or.jp/e/modules/tinyd00/content/images/12000/outlne03.jpg
[2] Image obtained online from: http://cyberparent.com/solar-electricity/images/cell-module-array.jpg

for monocrystalline, and between 9% and 12% for polycrystalline. For thin film cells, the efficiency is 10% for a Si, 12% for $CuInSe_2$ and 9% for CdTe [30]. Thus, the monocrystalline cell that has the highest efficiency was used in this work. A MATLAB/Simulink model of monocrystalline PV cell was carried out which made possible the prediction of the PV cell behaviour under varying solar irradiation.

3.3.2 Energy Performance

Solar arrays are designed to provide specific amounts of electricity under certain conditions. The following factors are usually considered when determining array energy performance:

- Characterization of solar cell electrical performance
- Determination of degradation factors related to array design and assembly
- Conversion of environmental considerations into solar cell operating temperatures
- Calculation of array power output capability.

The amount of electricity required may be defined by any one or a combination of the following performance criteria:

- Power output – power (W) available at the power regulator, specified either as peak power or average power produced during one day.
- Energy output – the amount of energy (Wh) produced during a certain period of time. The parameters are output per unit of array area (Wh/m²), and output per unit of array cost (Wh/€).
- Conversion efficiency – defined as "$(\frac{Power\ output\ from\ array}{Power\ input\ from\ sun}) \times 100\%$.

3.4 Classification of Wind Turbines

Wind turbine systems can be divided into two main groups based on the shaft orientation. These groups can be further subdivided by looking at rotor blade configuration or the number of blades and the way the turbine system is connected to the grid.

The two main groups of turbines consist of those with horizontal shaft configuration and those with vertical shaft configuration. As the names state, in the case of the horizontal shaft

configuration the shaft is in a horizontal position with the blade(s) connected to the one end of the shaft, as shown in Figure 3.3 (a) The vertical shaft wind turbine has a much longer shaft in a vertical position with the blades connected to the shaft at more than one point, as shown in Figure 3.3 (b).

The vertical shaft configuration turbines are further sub-categorised into groups by looking at the positioning and form of the blades. The most well-known vertical shaft wind turbine is Darrieus's phi-configuration, also known as the eggbeater configuration. Other well-known groups are the Musgrove, Diamond, Savonius, Giromill and Phi types [31, 32].

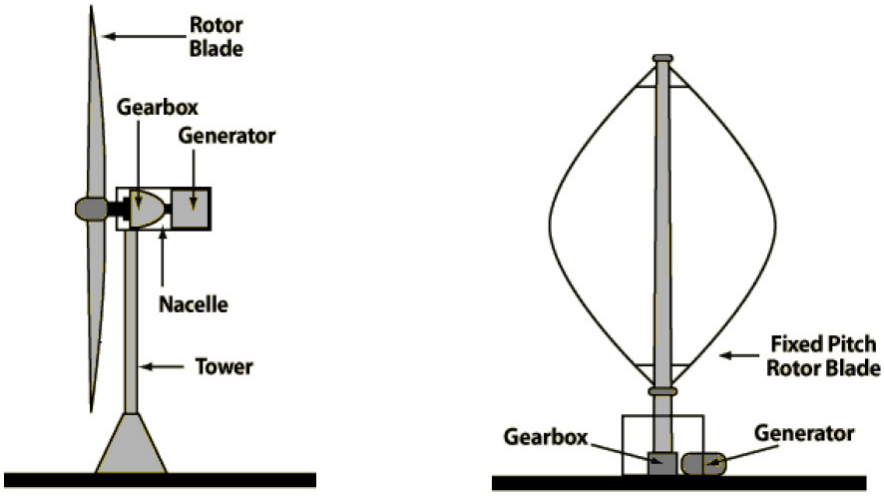

Figure 3.3 (a) Horizontal shaft configuration (left) (b) vertical shaft configuration (right) [33].

The biggest advantage of the vertical shaft wind turbine is the fact that it is omnidirectional, thus energy could be generated by wind blowing from any side without any adjustments needing to be made to the wind turbine. Such a configuration eliminates the need for yaw gears. Another advantage is that the generator and gearbox can be housed at ground level, leading to a simple and cheaper design, and most of the maintenance of the wind turbine can be done at ground level.

The major disadvantage of the vertical shaft wind turbine is the fact that these turbines are mostly not self-starting; additional mechanisms are required to start the wind turbine. Vertical shaft wind turbines are also known for lower efficiency as a result of the aerodynamically dead zones the blades need to pass through to complete their rotation [34].

Most modern wind turbine systems make use of the horizontal shaft configuration. This type of turbine configuration can be further subcategorised by looking at the number of turbine blades, which include single-blade, two-blade, three-blade, and multi-blade configurations. The advantages of having only a single blade are minimum drag losses and high ideal operation speed. High operation speed leads to a low-ratio gearbox which is cheaper. The disadvantages that stem from high operating speed are more wear and tear on the system and high noise emissions. Another disadvantage is that the blade needs to be balanced with a counter-weight. This weight does not contribute to the energy extracted but adds to drag losses. The single-blade configuration is unpopular because of problems with the balance, visual acceptability and high noise emission due to high aerodynamic loading and high speed [35].

As with the single-blade turbine, the two-blade turbine's ideal operating speed is high and, therefore, still quite noisy. The biggest disadvantage that turbines with an even number of blades have is that the uppermost blade gets maximum power from the wind at the exact time that the lowermost blade gets minimum power from the wind due to the influence of the tower. This results in stability problems in a machine or gearbox with a stiff structure. Consequently, turbines with an even number of blades are not used that often [34].

Since traditional manufacturers of two-blade turbines have switched to three-blade configurations, the three-blade upwind configuration is currently the most widely used commercial wind turbine [32, 34]. The three-blade turbine is also known as the classical Danish concept. This turbine provides greater dynamic stability than single- or two-blade turbines as they have an optically smoother operation, hence, visually integrating better into the landscape. All major manufacturers have three-blade turbine models available ranging from tens of kilowatt to as big as 6 MW [35]. After years of research by all the major turbine manufacturers, it seems that most have opted for the horizontal shaft configuration with three blades and situated upwind and this is the configuration which will be used in this thesis.

3.5 Energy Storage System

3.5.1 Introduction

There is currently considerable interest in electrical energy storage technologies for a variety of reasons. These include an ever increasing reliance on electricity in industry, the commercial sector and homes, the growth of renewable energy sources to meet the growing demand for electricity, and all combined with ever more stringent environmental requirements. The need of energy storage is to transfer the excess power during weak loads or excess supply from RESs to the peak periods [36]. The energy from the RESs has to be transformed into a storable energy form first and then transformed when storing is needed. This can be shown by the block diagram depicted in Figure 3.4.

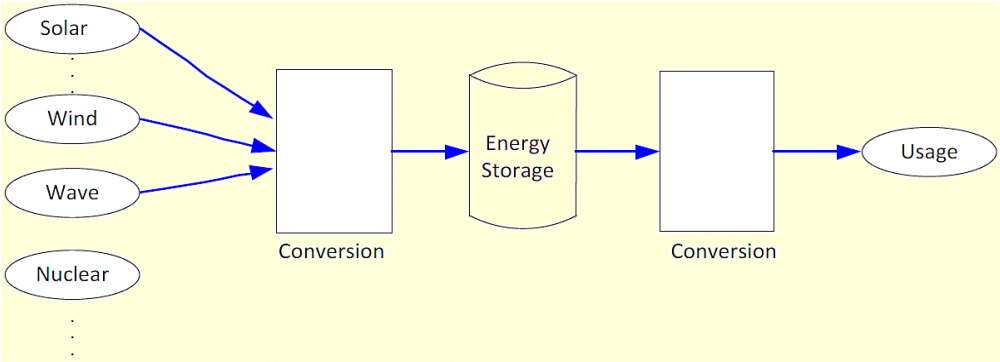

Figure 3.4 Energy storage with distributed energy generation system [2].

The energy storage techniques with hybrid power systems applied to the electrification of residential and remote sites will be discussed in this section.

The solar irradiation varies with time and so does the wind speed, throughout the day. Thus, in a hybrid wind-PV system, both the RESs and the load are fluctuating throughout the day. These fluctuations may result in imbalances in power distribution. As a result, the voltage and frequency in the power system will be affected. The addition of energy storage will assist balancing the distribution of power in the power network. The energy storage behaves like a large buffer to accommodate the unequal instantaneous energy in the power system. The energy storage element can act as a load or a generator depending on the supply to demand ratio [35-36]. There are many energy storage techniques. To mention some [35]:

- Battery Energy Storage System (BESS)
- Pumped Hydroelectric Storage System (PHSS)
- Superconducting Magnetic Energy Storage System (SMESS)
- Ultra-capacitors, etc.

The different energy storage techniques have different applications in power systems. Some of them are [35]:

a. Rapid reserve
b. Area control and frequency responsive reserve
c. Commodity storage
d. Transmission system stability
e. Transmission voltage regulation
f. Transmission and distribution facility deferral
g. Renewable energy management
h. Customer energy management
i. Power quality and reliability

Each technology has its own particular strengths and operational characteristics. In this thesis, the battery bank as energy storage device was considered for reasons discussed in Chapter 4.

3.5.2. Rechargeable Batteries

Battery bank is an electrochemical device which uses electrochemical reactions to store electricity in the form of potential chemical energy. The energy storing batteries used with wind-solar hybrid power systems are rechargeable in a sense that they can charge when there is enough supply from the RESs and discharge when there is larger load demand than there is supply [37].

Rechargeable batteries have standard electric potential which is the potential difference between the cathode and anode [38]. A simplified equivalent circuit of a battery at its steady state is shown below in Figure 3.5 working as a voltage source with an internal resistance.

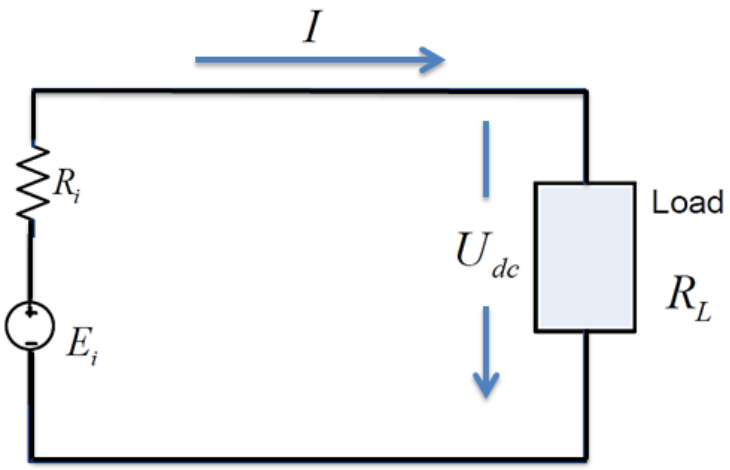

Figure 3.5 Simplified equivalent circuit of a battery.

The energy storage is dependent on the amount of active material in the battery cell [39]. Thus, for an active material of mass, m (in gram) and a cell volume, V (in litres), the specific power (in W/g) and peak power density (in W/l) can be determined from the peak power. Best batteries have high standard cell potential which results in high peak power capacity and high theoretical charge capacity [40].

3.5.3 Battery Characteristics

a) Battery Capacity

This is a measure of how much energy the battery can store. The amount of energy that can be extracted from a fully charged battery basically depends on temperature, rate of discharge, battery age and battery type. The three main ratings to specify the capacity of a battery are [40]:

- Ampere-hour (Ah): the current at which a battery can discharge at a constant rate over a fixed interval of time.
- Reserve capacity: the length of time (in minutes) that a battery can produce a specified level of discharge.
- kWh capacity: a measure of energy required to fully charge a depleted battery. A depleted battery is not usually a fully discharged battery.

b) Battery Voltage

The battery voltage is that of a fully charged battery. It depends up on the number of cells and voltage per cell. The battery voltage decreases when the battery starts discharging.

c) Cycle depth

Fully discharging batteries can facilitate the damage or totally destroy the battery life. Deep-cycle batteries can discharge up to 15%-20% of their capacity. This gives a depth of discharge of 85% - 80% [37].

d) Energy density

Energy density is a measure of how much energy can be extracted from a battery per unit of battery weight or volume. By default, deep-cycle batteries provide the potential for higher energy densities than non-deep-cycle varieties since more of the energy in the battery can be extracted.

e) Power density

Power density is a measure of how much power can be extracted from a battery per unit of battery weight or volume.

f) Durability (cycling capacity)

Energy storage system is designed to release the energy stored after each recharge in a fixed time. The number of times the energy storage can release the energy level it was designed for after each recharge is referred to as durability or cycling capacity. It is expressed in number of cycles, N_{cycles}. The cycling capacity mainly depends on the depth of discharge. The number of cycles versus the depth of discharge (DOD) of VRLA14 batteries is shown by Figure 3.6 below.

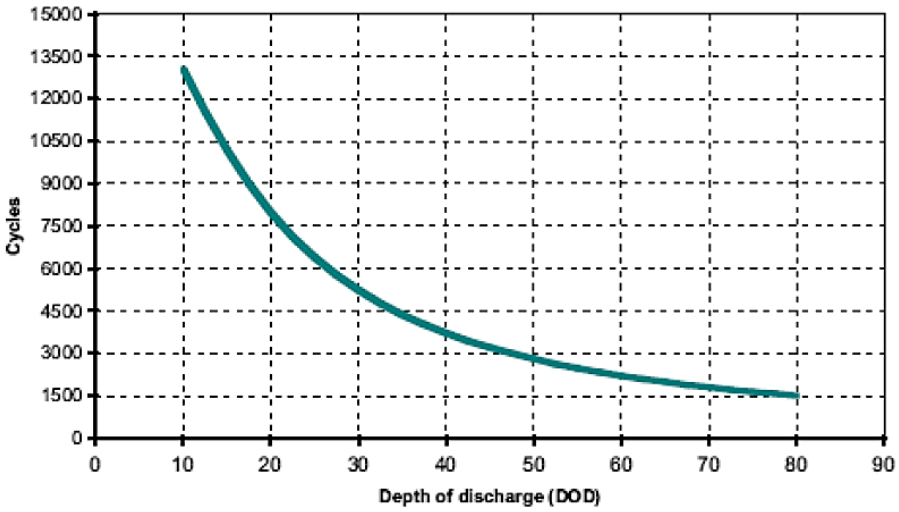

Figure 3.6 Cycling capacity vs. depth of discharge for lead-acid battery [40].

There are different types of batteries, but the most commonly used rechargeable batteries include [37, 41]:

- Lead acid battery
- Nickel cadmium (NiCad) battery
- Nickel metal hydride (NiMH) battery
- Lithium ion battery
- Lithium-polymer battery
- Zinc-air battery

4. Modelling and Implementation of Hybrid Wind-Solar Power Generator System in Simulink

4.1 Full-Model Architecture

The system discussed in this project is a 4.1 kW wind-solar hybrid system with energy storage capability. The system comprises a 1.6 kW PV array which is connected to a boost DC-DC converter that is controlled by a Perturb and Observe (P&O) algorithm block implemented for maximum power point tracking (MPPT), then a 2.5 kW grid-connected wind turbine which uses a PMSG with generator- and grid-side controller and converter topology and is connected to a bidirectional boost-buck converter, and finally a battery bank - connected to a bidirectional DC-DC converter – used for energy storage. The schematic diagram of the proposed system architecture is shown in Figure 4.1.

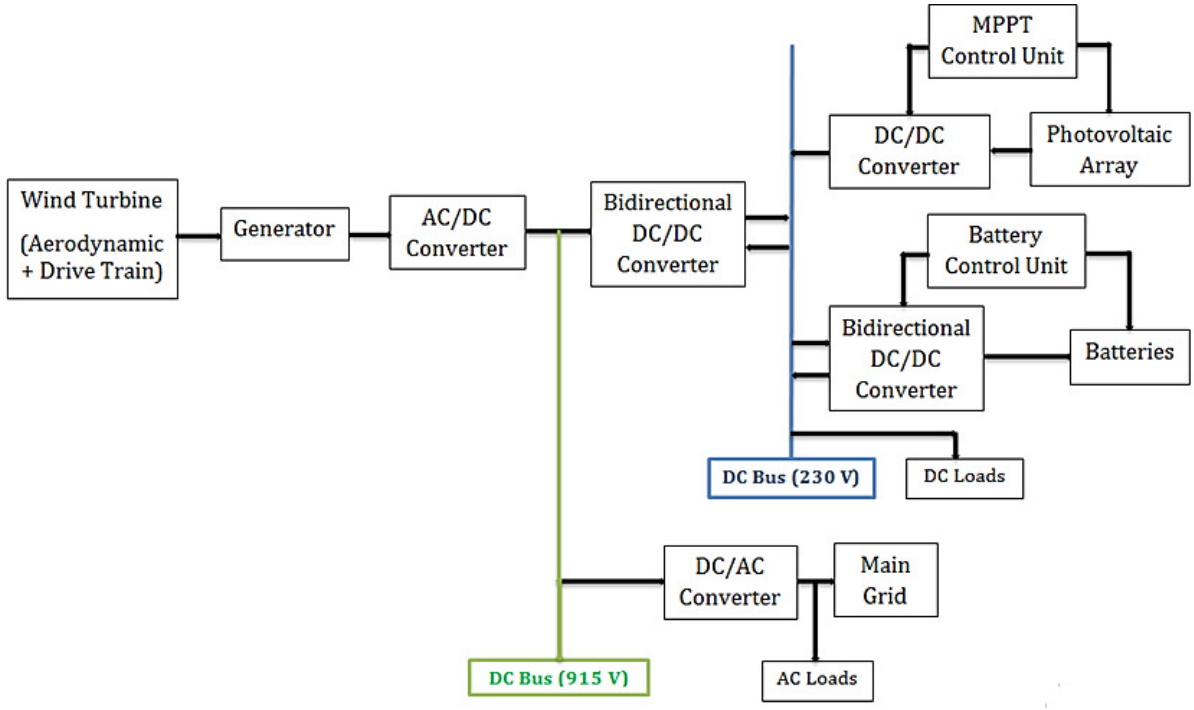

Figure 4.1 Wind-solar hybrid power generator system architecture.

In the proposed system, the wind turbine first converts the kinetic energy of the wind to mechanical energy of the turbine blades and finally converts this to electricity. In terms of its

physical structure, the wind turbine consists of a tower, an alternator, and a propeller (blades). The kinetic energy of the wind is converted to the mechanical energy in the rotor, and then transmitted to the PMSG where the rotor shaft speed is accelerated without the need for a gearbox. The electricity that comes from the PMSG goes to a bidirectional DC-DC converter, and can then get stored in the batteries, or sent to the grid through an inverter. The solar panels in the system convert solar radiation directly to electricity.

Finally, the battery module used is a 15 Ahr, 96 V (which is equivalent to four 24 V batteries) Lead-acid to feed the DC loads. The system is designed in such a way that the wind turbine and the PV system will feed the battery through a bidirectional DC-DC converter to meet the DC load requirement and the wind turbine will provide AC power to the grid.

4.2 PV System

The PV array used in the proposed system consists of PV modules which consist of solar PV cells. The general mathematical model for the solar cell has been studied over the past three decades [42]. The circuit for the solar cell model, which includes a current source, a diode, a parallel resistor, R_{sh}, and a series resistor R_s, is shown in Figure 4.2.

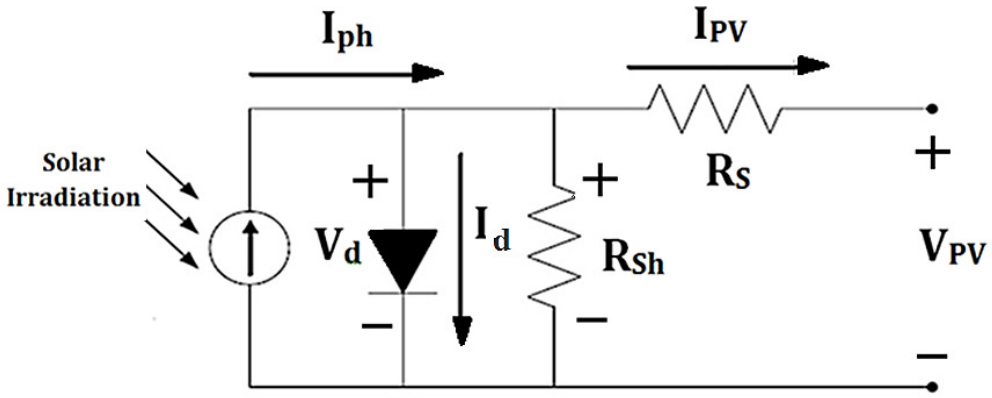

Figure 4.2 Equivalent circuit of a PV cell.

According to the PV cell circuit shown in Figure 4.2 and Kirchhoff's Current Law (KCL), the photovoltaic current, I_{PV} can be presented as follows [30]:

$$I_{PV} = I_{ph} - I_d \left[e^{\left(\frac{qV_d}{NKTc}\right)} - 1 \right] - \frac{(V_{PV} + R_s I_{PV})}{R_{sh}} \quad (4.1)$$

where, I_{ph} is the photocurrent, I_d is the reverse saturation current of the diode, q is the electric charge = 1.6×10^{-19} C, V_d is the voltage across the diode, K is Boltzmann's constant = 1.38×10^{-23} J/K, T_c is the absolute temperature of the PV cell, N is the ideality factor of the diode - which is a measure of how closely the diode follows the ideal diode equation (where $N = 1$ means that the diode follows the ideal diode equation perfectly [43]), V_{PV} is the photovoltaic voltage, R_s is the series resistor = 1 mΩ, and R_{sh} is the shunt resistor = 1 kΩ.

Based on equation 4.1, the Simulink model of the PV cell depicted in Figure 4.2 was developed in Simulink using circuit components from the SimPowerSystems library as shown in Figure 4.3. The diode used in this model is controlled by its own voltage V_{ak}. When the diode is forward biased ($V_{ak} > 0$), it starts to conduct with a small forward voltage V_f across it (where V_f = 0.6 V). It turns off when the current flow into the device becomes 0. When the diode is reverse biased ($V_{ak} < 0$), it stays in the off state.

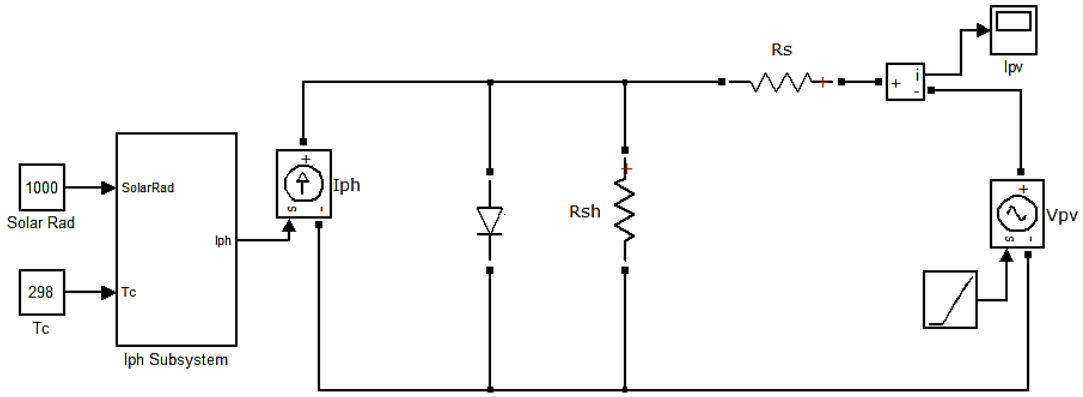

Figure 4.3 Simulink model of a PV cell.

In equation 4.1 (and also in the subsystem shown in Figure 4.3), the photocurrent, I_{ph} mainly depends on solar irradiation and ambient temperature as shown by equation 4.2 [44]:

$$I_{ph} = [I_{sc} + K_i(T_c - 298)] \frac{G}{1000} \quad (4.2)$$

where K_i = 0.0017 A/°C is the cell's short circuit current temperature coefficient, I_{sc} is the short-circuit current= 9.1 A, and G is the variable solar radiation (W/m^2). Based on equation 4.2, the subsystem for I_{ph} of Figure 4.3 is shown in Figure 4.4.

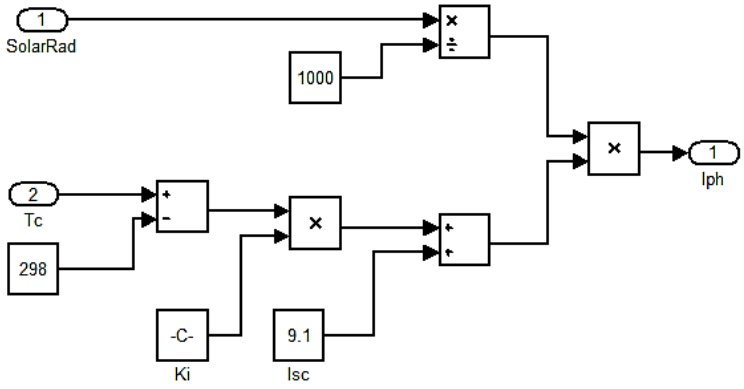

Figure 4.4 Simulink model for the PV photocurrent, I_{ph}.

Based on Figure 4.4 the effect of varying solar irradiation on the photocurrent for a constant cell's absolute temperature, T_c = 303 K was observed. The simulation result was plotted as shown in Figure 4.5.

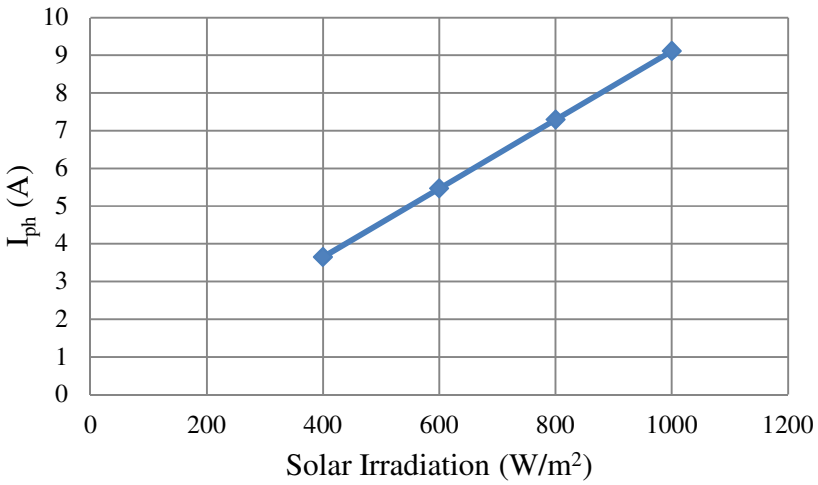

Figure 4.5 Solar irradiation versus PV photocurrent.

In order to observe the effect of varying solar irradiation on the PV cell's current and voltage, namely I_{PV} and V_{PV} from equation 4.1, the model in Figure 4.3 was simulated for a constant cell's absolute temperature, T_c = 298 K and the results were plotted as shown in Figure 4.6.

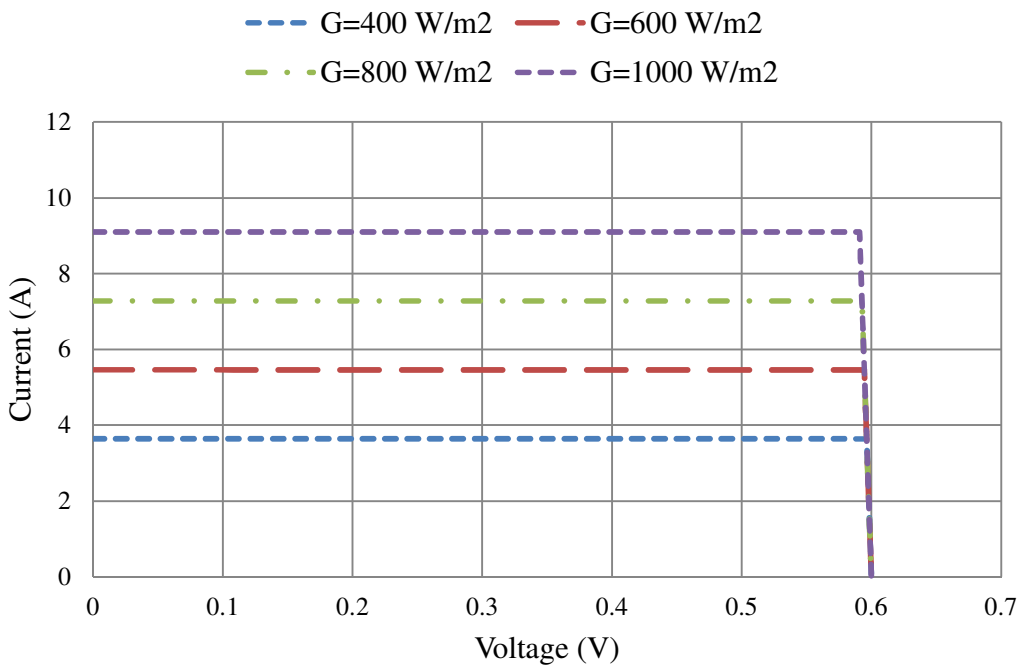

Figure 4.6 V-I graphs for various solar irradiations for a PV cell.

The power produced by a PV cell, P_{PV}, is calculated using equation 4.3:

$$P_{PV} = I_{PV} \times V_{PV} \tag{4.3}$$

Since there is a direct relationship between the PV voltage and its output power, by incrementing the photocurrent the output power also changes due to variations in the voltage as depicted in Figure 4.7.

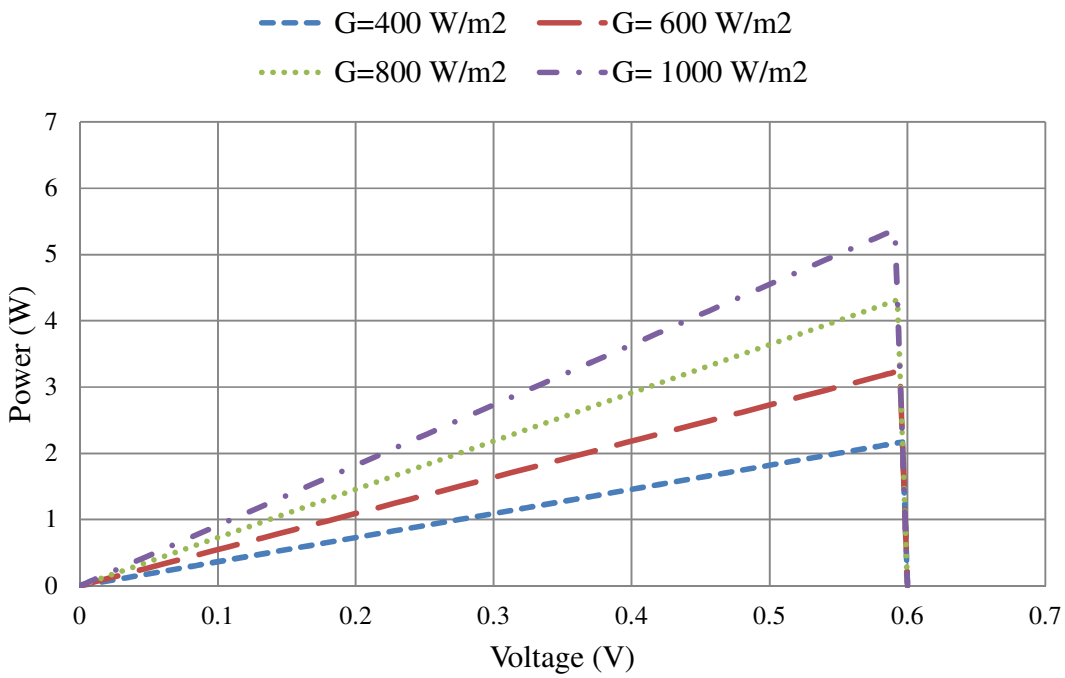

Figure 4.7 V-P graphs for various solar irradiations for a PV cell.

It was found from Figure 4.6 and 4.7 that with increased solar irradiance there is an increase in both the maximum power output and the short circuit current.

As previously mentioned, a PV module is a connection of many PV cells. In this model, 30 PV cells were interconnected in series to form one module. As a result, the module's voltage was obtained by multiplying the single cell open circuit voltage by the number of cells while the total module current was equivalent to that of a single cell's (in this case, the module had a total open circuit voltage of $30 \times 0.6\ \text{V} = 18\ \text{V}$ and a short circuit current of 9.1 A).

Afterwards, 10 PV modules were interconnected in series to form a PV array with a total open circuit voltage of 180 V. The V-I and V-P simulation results for T_c = 303 K and solar irradiation values of 400-1000 W/m^2 are depicted in Figure 4.8 and 4.9.

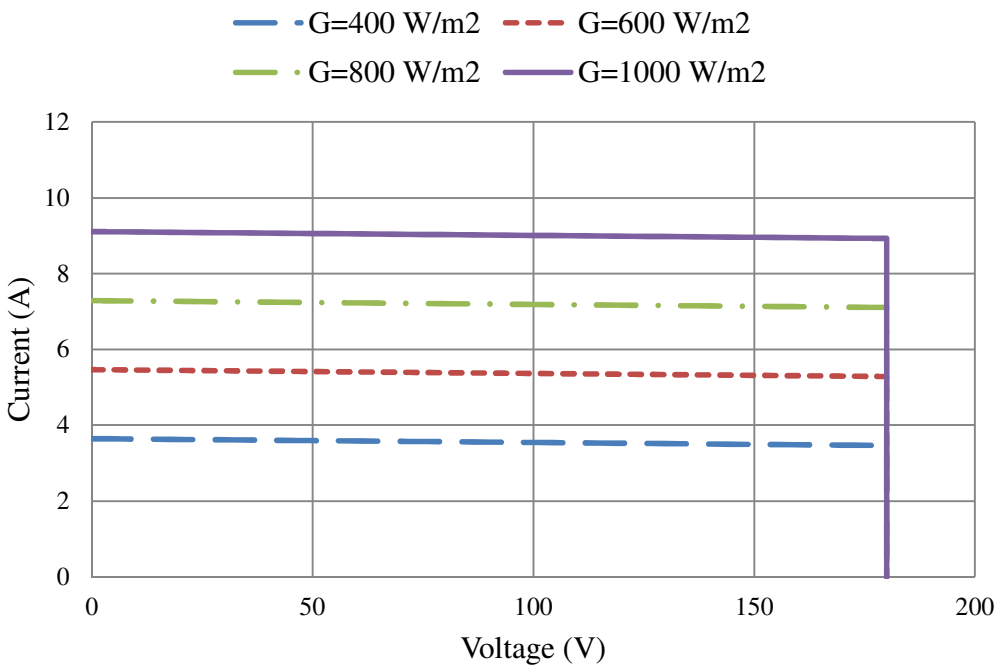

Figure 4.8 V-I curve of the PV array.

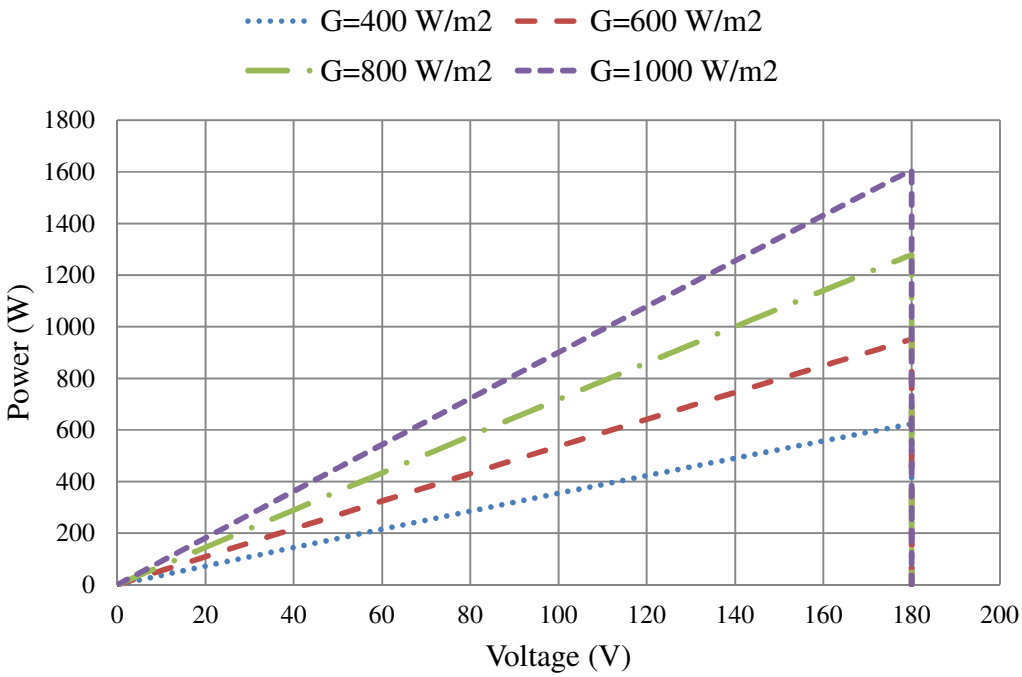

Figure 4.9 V-P curve of the PV array.

4.2.1 Solar Array Boost DC-DC Converter

In power systems, converters are circuits consisting of semiconductor devices operated as (near-ideal) switches, capacitors and magnetic components (e.g. inductors) that are connected in a topology such that in order to produce the desired DC conversion, the periodic switching controls the dynamic transfer of power from the input to the output. The storage elements in these converters are connected in such a way that they form a low-pass filter to yield a low output ripple voltage [45].

A boost or a step-up DC-DC converter is a power converter which produces an output voltage greater than its input voltage or in other words, "steps-up" the source voltage. It usually includes two nearly-ideal semiconductor switches (such as a diode and a transistor/metal-oxide semiconductor field effect transistor (MOSFET)) and also an energy storage element such as a capacitor, an inductor or the two in combination. Filters made of capacitors (sometimes in combination with inductors or resistors) are normally added to the output of the converter to reduce output voltage ripple. Since power is conserved, the output current of these converters is lower than their input current. Figure 4.10 depicts the configuration of a boost DC-DC converter.

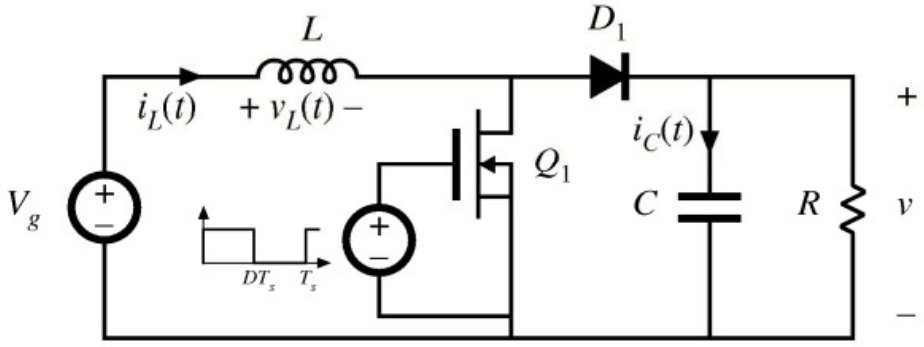

Figure 4.10 Boost DC-DC converter with realisation of ideal switches (MOSFET and diode).

What drives the boost converter is the tendency of the inductor to resist changes in current by creating and destroying a magnetic field. Two states exist in the configuration as shown in Figure 4.11 (a) and (b) [46].

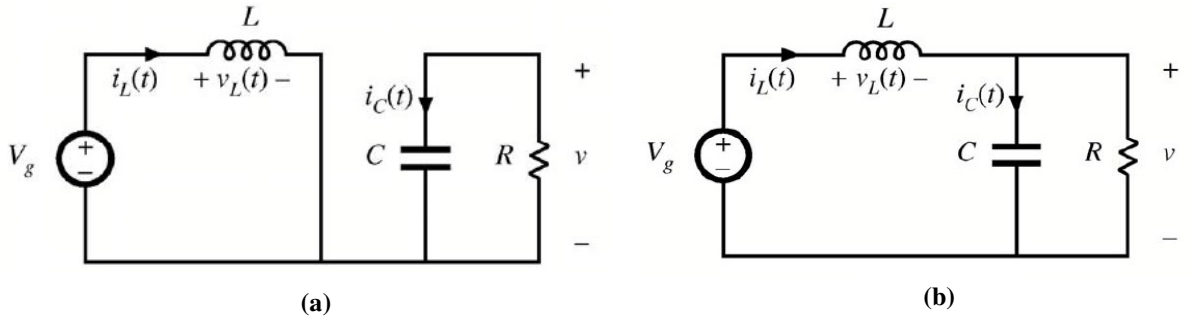

Figure 4.11 Switching modes of the DC-DC converter circuit.

(a) When the switch is in position 1 as Figure 4.11 (a) shows, current flows through the inductor in clockwise direction and the inductor stores some energy by generating a magnetic field. In this case, the inductor voltage and capacitor current are formulated as shown in equations 4.4 and 4.5 respectively.

$$v_L = V_g \tag{4.4}$$

$$i_c = -v/R \tag{4.5}$$

(b) When the switch is in position 2 as shown in Figure 4.11 (b), current will be reduced since the impedance is higher. The magnetic field previously created will be obliterated in order to maintain the current flow towards the load. Equations 4.6 and 4.7 formulate the described state:

$$v_L = V_g - v \tag{4.6}$$

$$i_c = i_L - v/R \tag{4.7}$$

The inductor voltage, v_L and capacitor current, i_c waveforms for equations 4.6 and 4.7 are depicted in Figure 4.12.

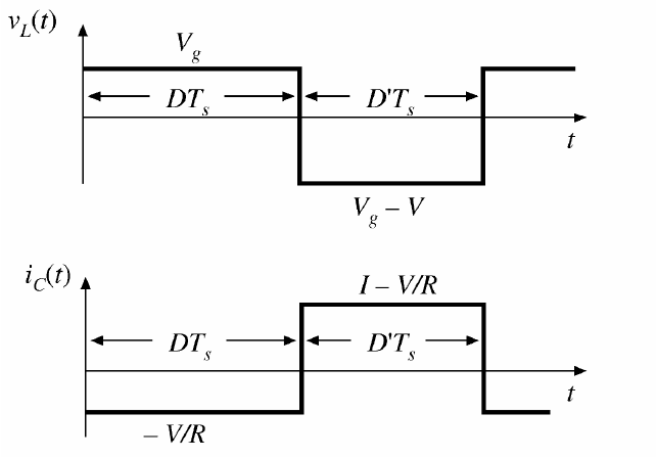

Figure 4.12 Boost DC-DC converter inductor voltage and capacitor waveform.

where, D is the duty cycle and $D' = 1 - D$. The waveforms show a periodic steady-state operation, where the inductor's average inductor voltage = 0V and the average capacitor current = 0A.

If the switch is cycled at a fast speed, the inductor will not be able to discharge fully in between the charging stages and hence, the load experiences a voltage greater than that of the input source alone when the switch is in position 2. Also, while the switch is in position 2, the capacitor, C in parallel with the load, R is charged to this combined voltage. When the switch is then in position 1 and the right hand side of the circuit is shorted out from the left hand side, the capacitor is then able to provide the voltage and energy to the load resistance. It should be noted that the switch must be opened again fast enough to prevent the capacitor from discharging too much [47].

In order to implement the boost DC-DC switching circuit, the following relations should be noted for the inductor voltage, v_L.

The net volt-seconds applied to the inductor over one switching period is:

$$\int_0^{T_s} v_L(t)dt = \big(V_g\big)DT_s + \big(V_g - V\big)D'T_s \tag{4.8}$$

Equating this to zero and collecting the terms results in the following:

$$V_g(D + D') - VD' = 0$$

Solving the above equation for V gives:

$$V = \frac{V_g}{D'} \tag{4.9}$$

The boost DC-DC converter steps-up its DC input voltage by a ratio known as the voltage conversion ratio, $M(D)$ which is electronically adjustable by changing the switch duty cycle D as shown in equation 4.10 [47].

$$M(D) = \frac{V}{V_g} = \frac{1}{D'} = \frac{1}{1-D} \tag{4.10}$$

Based on the developments so far, the Simulink model for the DC-DC circuit was built and connected to the PV system as shown in Figure 4.13.

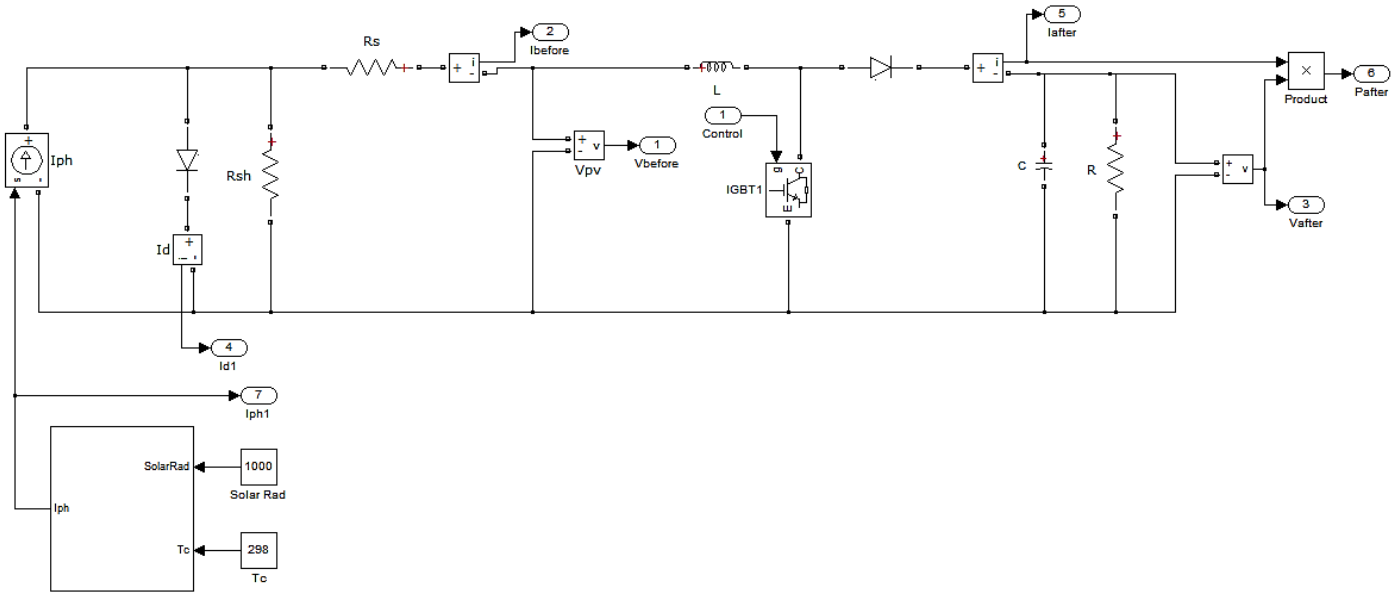

Figure 4.13 DC-DC converter Simulink model.

4.2.2 Maximum Power Point Tracking

During certain times of the day, there is a mismatch of sunlight radiation and so, partially shaded conditions occur for PV systems which can significantly affect the output power generated by the system. This phenomenon thereafter affects the V-P curve of PV arrays, which makes the maximum power point (MPP) very difficult to accomplish. Therefore, a maximum power point

tracking (MPPT) technique is needed to operate the PV module at its MPP. Thus, the objective of the MPP tracking algorithm is to adjust the DC-DC control variable so that the PV array operates at the maximum power point [48].

A perturb and observe (P&O) algorithm is the MPPT control algorithm that can be adapted to the model. In the case of a PV array connected to a boost DC-DC converter, perturbing the duty ratio of the power converter perturbs the PV array current and consequently perturbs the PV array voltage. The algorithm reads or "observes" the value of current and voltage from the PV array. Power is then calculated from the observed voltage and current using equation 4.3. The value of voltage and power at k^{th} instant are stored. Then, the next values at the $(k+1)^{th}$ instant are observed again and power is calculated from the observed values. The power and voltage at the $(k+1)^{th}$ instant are subtracted from the values at the k^{th} instant. By studying the V-P curve of the PV array, it is clear that the right side of curve where the voltage is almost constant, the slope of the V-P curve is negative ($dP/dV < 0$) whereas in the left side of the curve the slope is positive ($dP/dV > 0$). The right side of the V-P curve is the lower limit for the duty cycle (close to zero) whereas the left side of the curve is the upper limit for the duty cycle (close to unity). Depending on the sign of $dP(P(k+1) - P(k))$ and $dV(V(k+1) - V(k))$, after subtraction, the algorithm decides whether to increase the duty cycle or to reduce it [49]. The flow chart of the P&O algorithm is presented in Figure 4.14. The implementation of this algorithm in Simulink is depicted in Figure 4.15.

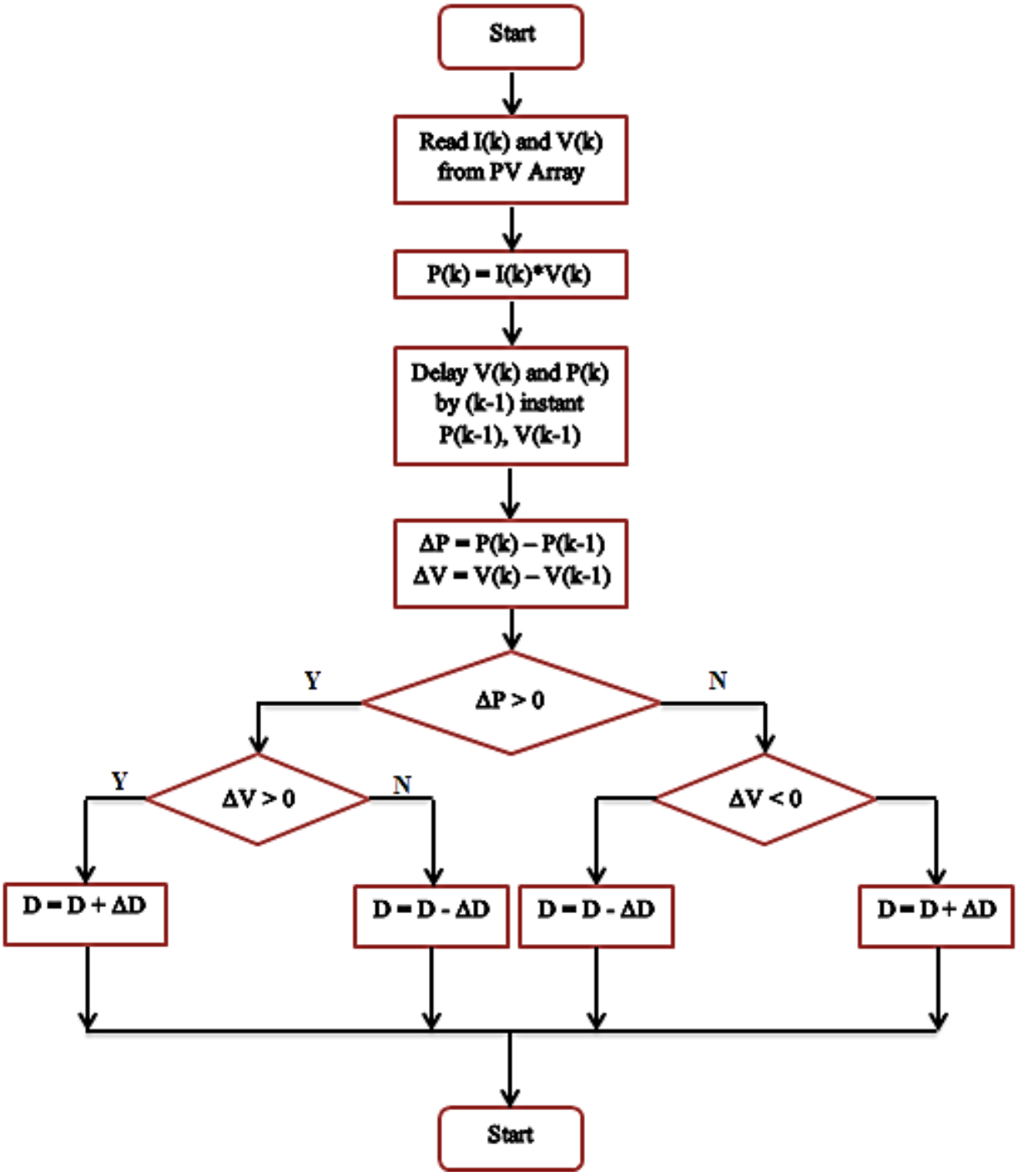

Figure 4.14 P&O algorithm flowchart.

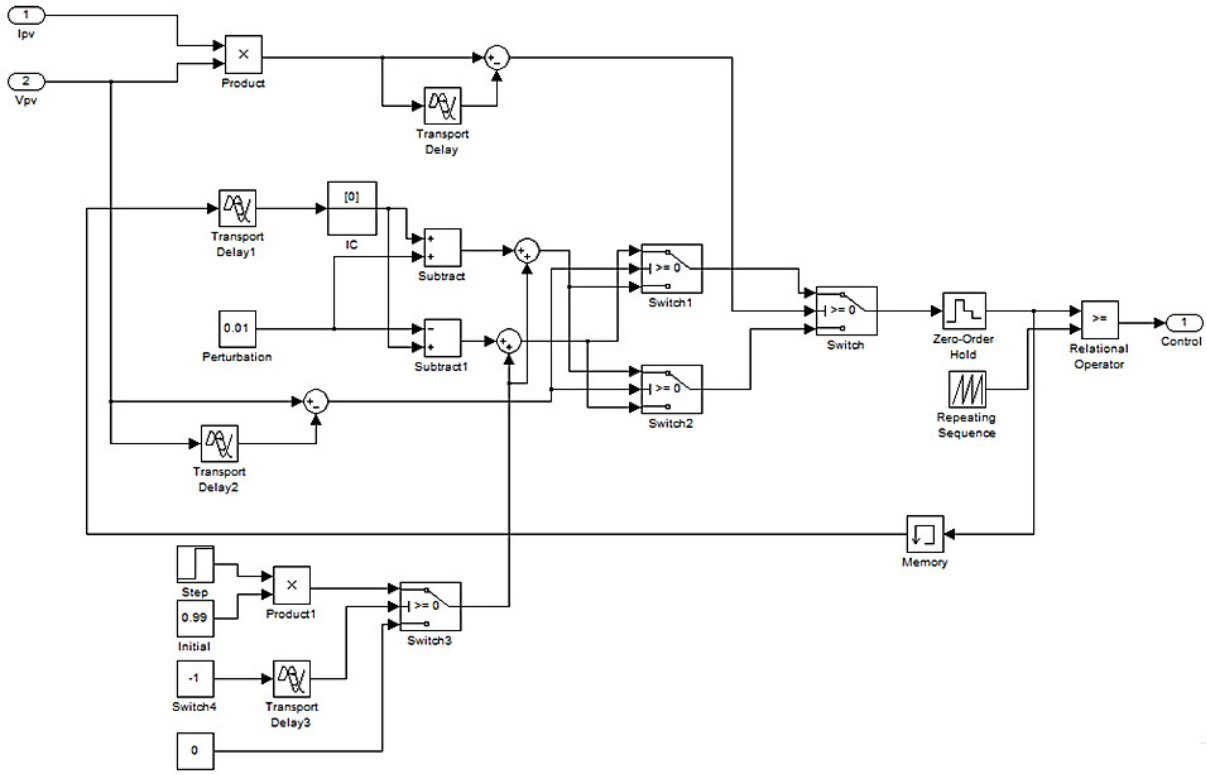

Figure 4.15 Implementation of MPPT algorithm in Simulink.

Having now developed the required model and controller system/algorithm for the boost DC-DC converter, the MPPT block can be implemented together with the PV array and the boost DC-DC converter as shown in Figure 4.16.

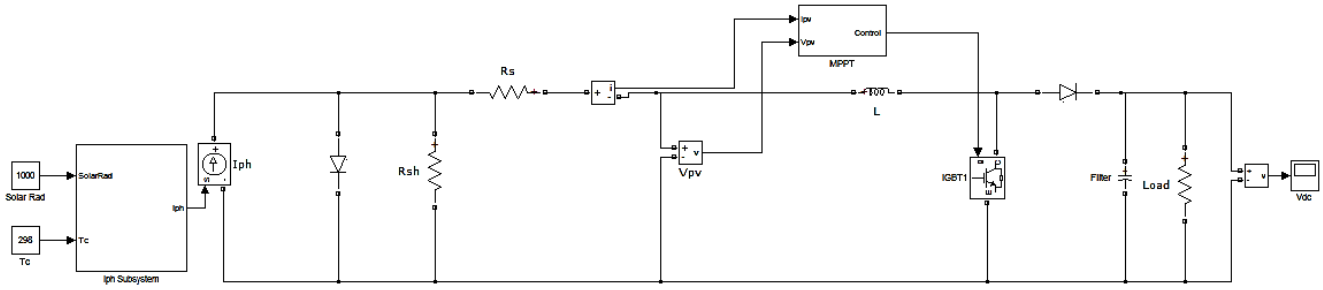

Figure 4.16 PV array connected to a boost DC-DC converter and MPPT controller.

The simulation result for the output current, voltage and power of the PV system (for $G = 1000$ W/m^2 and $T_c = 303$ K) where the PV array is connected to the boost DC-DC converter and controlled by the MPPT algorithm is depicted in Figure 4.17-4.19. In these figures, some noise

can be observed. This is because when the steady state is reached in the system, the algorithm oscillates around the peak point and so some noise is introduced to the outputs.

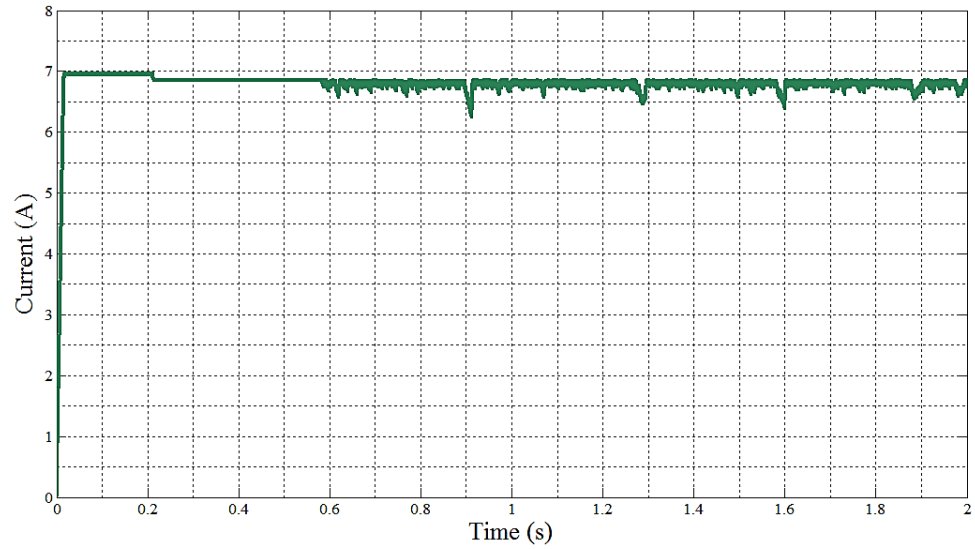

Figure 4.17 Output current of PV array + boost DC-DC converter.

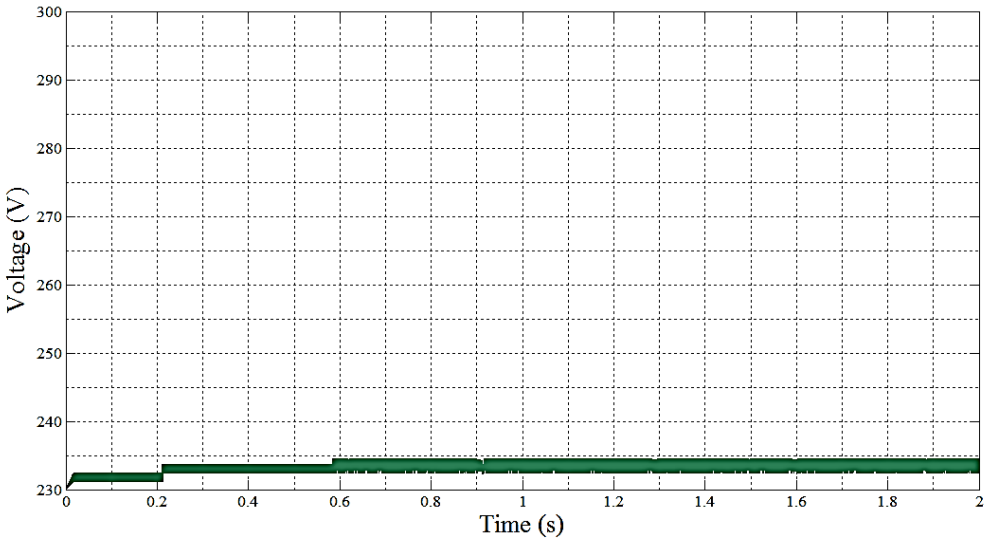

Figure 4.18 Output voltage of PV array + boost DC-DC converter.

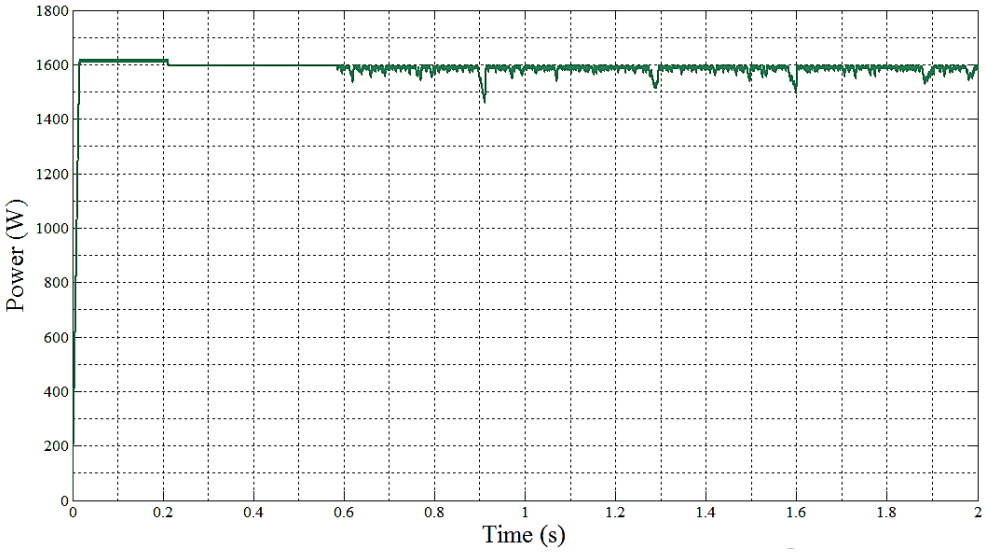

Figure 4.19 Output power of PV + boost DC-DC converter.

4.3 Wind Turbine System

The system analysed in this section is a wind turbine driven by a direct-driven (gearless) PMSG. The generator is connected to the grid via an AC-DC-AC converter, which consists of a controlled generator-side converter, a DC-link modelled as a capacitor, a controlled grid-side converter, and a bidirectional DC-DC converter. The layout of the overall wind turbine model is depicted in Figure 4.20.

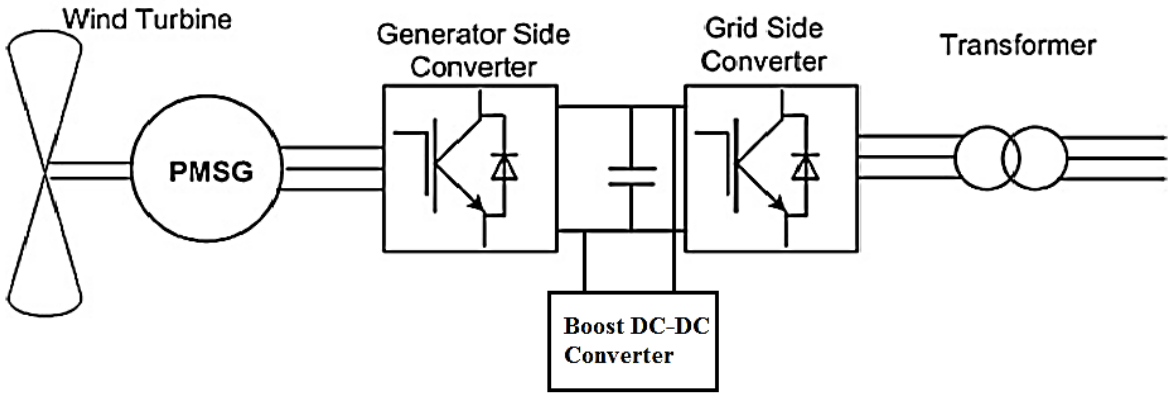

Figure 4.20 Electrical scheme of a variable speed wind turbine equipped with a direct-driven PMSG.

4.3.1 Wind Turbine Module

The first part of the proposed system depicted in Figure 4.20 is the wind turbine module, which is used to convert the wind's kinetic energy into mechanical work. The model used is based on the steady-state power characteristics of the turbine. The friction factor and the inertia of the turbine must be combined with those of the generator coupled to the turbine. The output power of the turbine is given by equation 4.11 [50].

$$P_m = c_p(\lambda, \beta)\frac{\rho A}{2}v_{wind}^3 \tag{4.11}$$

Where, P_m is the mechanical output power of the turbine (W), c_p is the performance coefficient of the turbine, ρ is the air density (kg/m^3), A is the turbine swept area (m^2), v_{wind} is the wind speed (m/s), λ is the tip speed ratio of the rotor blade tip speed to wind speed, and β is the blade pitch angle (degrees).

The rotor torque T_w of the wind turbine can now be computed as:

$$T_w = \frac{P_m}{\omega_m} = \frac{c_p(\lambda, \beta)\frac{\rho A}{2}v_{wind}^3}{\omega_m} \tag{4.12}$$

where ω_m is the angular velocity of the rotor (rad/s).

Equation 4.11 can be normalised and converted to per unit (pu) system as shown below:

$$P_{m\_pu} = k_p c_{p\_pu} v_{wind\_pu}^3 \tag{4.13}$$

where, P_{m_pu} is the power in pu of the nominal power for particular values of ρ and A, c_{p_pu} is the performance coefficient in pu of the nominal maximum value of c_p, v_{wind_pu} is the wind speed in pu of the base wind speed (the base wind speed is the mean value of the expected wind speed in m/s), and k_p is the power gain for $c_{p\_pu} = 1$ pu and $v_{wind\_pu} = 1$ pu (k_p is less than or equal to 1). A generic equation is used to model $c_p(\lambda, \beta)$. This equation, based on the modelling turbine characteristics of [51], is:

$$c_p(\lambda, \beta) = c_1(c_2/\lambda_i - c_3\beta - c_4)e^{-c_5/\lambda_i} + c_6\lambda \tag{4.14}$$

where,

$$\frac{1}{\lambda_i} = \frac{1}{\lambda + 0.08\beta} - \frac{0.035}{\beta^3 + 1} \tag{4.15}$$

The coefficient c_1 to c_6 are: $c_1 = 0.5176,\ c_2 = 116,\ c_3 = 0.4,\ c_4 = 5, c_5 = 21,$ and $c_6 = 0.0068$. The c_p-λ characteristics for different values of the pitch angle β are illustrated in Figure 4.21. The maximum value of c_p ($c_{pmax} = 0.48$) is achieved for $\beta = 0$ degree and for $\lambda = 8.1$. This particular value of λ is defined as its nominal value (λ_{nom}).

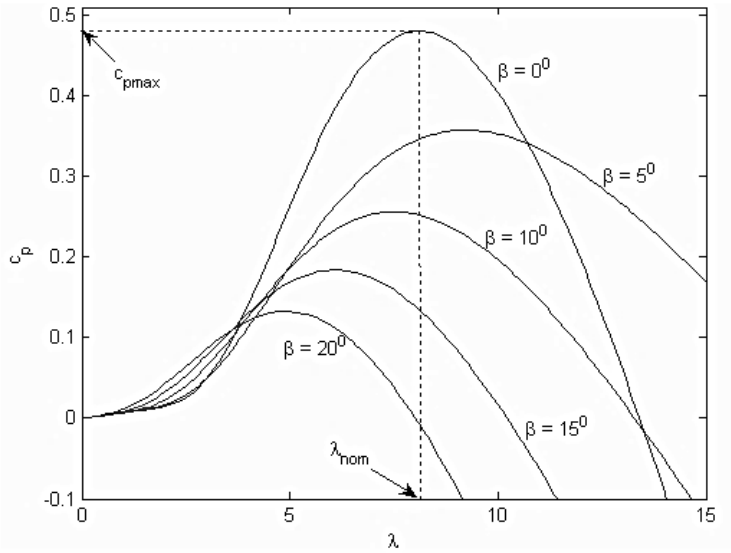

Figure 4.21 c_p-λ curves for different values of the pitch angle, β.

The Simulink model of the turbine is illustrated in Figure 4.22. The three inputs are the generator speed, ω_{r_pu} (in pu of the nominal speed of the generator), the pitch angle in degrees and the wind speed in m/s. The tip speed ratio λ in pu of λ_{nom} is obtained by the division of the rational speed in pu of the base rotational speed and the wind speed in pu of the base wind speed [51]. The output is the torque applied to the generator shaft. Figure 4.23 shows the simulation result of the wind turbine module for output power.

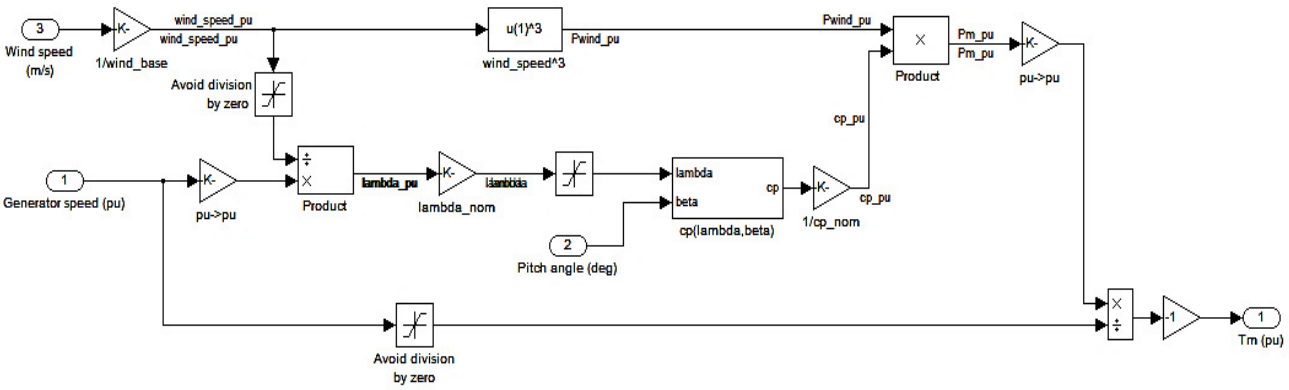

Figure 4.22 Model of wind turbine in Simulink.

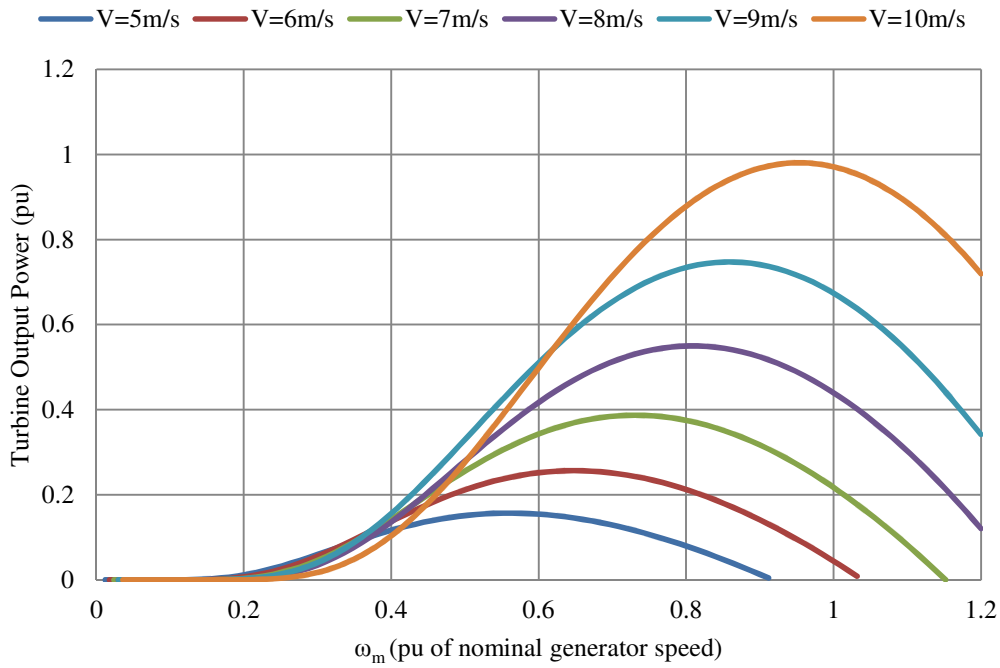

Figure 4.23 Horizontal turbine output power for different wind speeds.

As depicted in Figure 4.23, wind speed is the most influential factor on the amount of power produced by the wind turbine. Because the power in the wind is a cubic function of wind speed, changes in speed produce a profound effect on the output power.

4.3.2 Permanent Magnet Synchronous Generator

The PMSG has been considered as a system which makes possible to produce electricity from the mechanical energy obtained from the wind. The advantages of PMSG over induction

machines are its high efficiency and reliability, since they do not require an additional DC supply for the excitation circuit, their smaller size and being easy to control [52]. Of course PMSGs have a number of disadvantages too such as higher costs due to the use of large magnets and some structural and thermal issues. However, over the years the PMSG has become a more attractive solution to use in numerous wind turbine applications.

In this thesis, the permanent magnet synchronous machine (PMSM) from the SimPowerSystems library was used. The PMSM block operates in either generator or motor mode. The mode of operation is dictated by the sign of the mechanical torque (positive for motor mode, negative for generator mode). The sinusoidal model assumes that the flux established by the permanent magnets in the stator is sinusoidal, which implies that the electromotive forces are sinusoidal.

The equations used for the PMSG are expressed in the rotor reference frame (qd frame). All quantities in the rotor reference frame are referred to the stator [53].

$$\frac{d}{dt}i_{sd} = \frac{1}{L_{sd}}v_{sd} - \frac{R}{L_{sd}}i_{sd} + \frac{L_{sq}}{L_{sd}}p\omega_r i_{sq} \tag{4.16}$$

$$\frac{d}{dt}i_{sq} = \frac{1}{L_{sq}}v_{sq} - \frac{R}{L_{sq}}i_{sq} + \frac{L_{sd}}{L_{sq}}p\omega_r i_{sd} - \frac{\lambda p\omega_r}{L_{sq}} \tag{4.17}$$

$$T_e = 1.5p[\lambda i_{sq} + (L_{sd} - L_{sq})i_{sd}i_{sq}] \tag{4.18}$$

where L_{sq} and L_{sd} are the q and d axis inductances respectively, R is the resistance of the stator windings, i_{sq}, i_{sd}, v_{sq} and v_{sd} are the q and d axis current and the q and d axis voltages respectively, ω_r is the angular velocity of the rotor, λ is the amplitude of the flux induced by the permanent magnets of the rotor in the stator phase, and p is the number of pole pairs.

In surface-mounted PMSGs, $L_d = L_q$, hence, the electromagnetic torque can be rewritten as follows:

$$T_e = 1.5p\lambda i_{sq} \tag{4.19}$$

4.3.3 Interfacing Converters

As shown in Figure 4.20 in variable speed wind turbines, PMSG is connected to the main power grid via a 3-phase back-to-back set of converters. The first converter, namely the generator-side converter is connected to the stator windings of the PMSG. While the other one is known as the grid-side converter and is connected to the grid via an AC filter. The DC terminals of the two converters are connected together with a shunt DC capacitor. Control schemes of the two converters will be explained in detail in the following sections.

The grid-side and generator side converters are implemented using the Universal Bridge block from the SimPowerSystems library which implements a universal three-phase power converter that consists of up to six power switches connected in a bridge configuration. The type of power switch and converter configuration used is selectable from the dialog box. For the proposed system, the IGBT-diode bridge configuration was used for both the generator-side and the grid-side interface as shown in Figure 4.24:

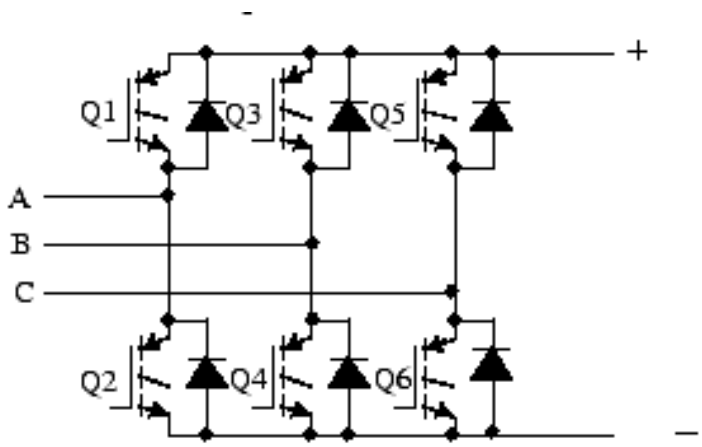

Figure 4.24 IGBT-diode bridge configuration.

4.3.3.1 Generator-Side Converter Control

For the generator side, the voltage equations of the PMSG can be expressed in the synchronous qd reference frame as shown below:

$$v_{sd} = Ri_{sd} + L_{sd}\frac{d}{dt}i_{sd} - \omega_r L_{sd} i_{sq} \tag{4.20}$$

$$v_{sq} = Ri_{sq} + L_{sq}\frac{d}{dt}i_{sq} + \omega_r L_{sd} i_{sd} + \omega_r \lambda \tag{4.21}$$

The generator-side controller is mainly used to control the wind turbine shaft speed in order to maximize the output power. In a variable speed wind energy conversion system, the maximum power at different wind speeds depends on the power coefficient, c_p. Generally, for wind turbines, c_p is not constant. The parameters affecting c_p include: the tip speed ratio λ and the pitch angle β as illustrated in Figure 4.21. To obtain the maximum power, P_{max} from the wind turbine, the turbine should operate at c_{p_max} and hence, it is necessary to keep the generator rotor speed ω_m to meet the optimum value of the tip speed ratio, λ_{opt}. If the wind speed varies, the rotor speed should be adjusted to follow the change of the wind speed [54]. The generator speed control is typically accomplished through the generator-side converter. Hence, the control of the generator-side converter allows the generator to tune the rotational speed depending on the incident wind variation. To understand the control concept, the equation of motion for a generator should be discussed as shown below [55]:

$$J\frac{d\omega_m}{dt} = T_m - T_e - B\omega_m \tag{4.22}$$

where J is the inertia of the whole system including the turbine and generator (Kgm^2), and B is the friction factor (Nms).

Based on equation 4.22, the generator rotational speed is governed by the electromagnetic torque and hence speed control is obtained by generator torque control. From equation 4.19, the electromagnetic torque may be controlled directly by q-axis current component, i_{sq}, and hence, the speed can be controlled by changing the q-axis current component. The d-axis current component i_{sd} is set to zero to minimize the current flow for a given torque, and thus minimizes the resistive losses [56]. The stator voltage components, v_{sd}, and v_{sq}, synthesised by the generator-side converter can be employed to govern the generator current components i_{sd} and i_{sq}, as seen in equations 4.22 and 4.23. The controller requires feedback from the PMSG stator current components, i_{sq}, and i_{sd}. The error between measured and reference components is the input of PI controller [57]. Then, the compensation terms shown in equations 4.20 and 4.21 are

considered to ensure stable and decoupled active and reactive power control as shown in Figure 4.25.

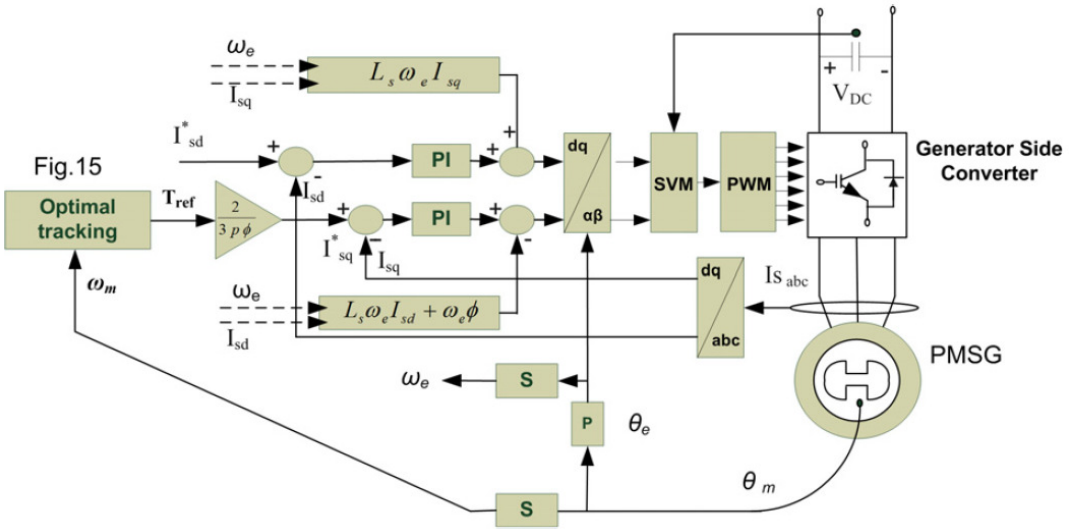

Figure 4.25 Block diagram of the generator-side converter control.

Based on the control strategy and equations described and the block diagram of Figure 4.25, the Simulink model for the generator-side control system was designed as shown in Figure 4.26. Figure 4.27 shows the overall Simulink block of the control system.

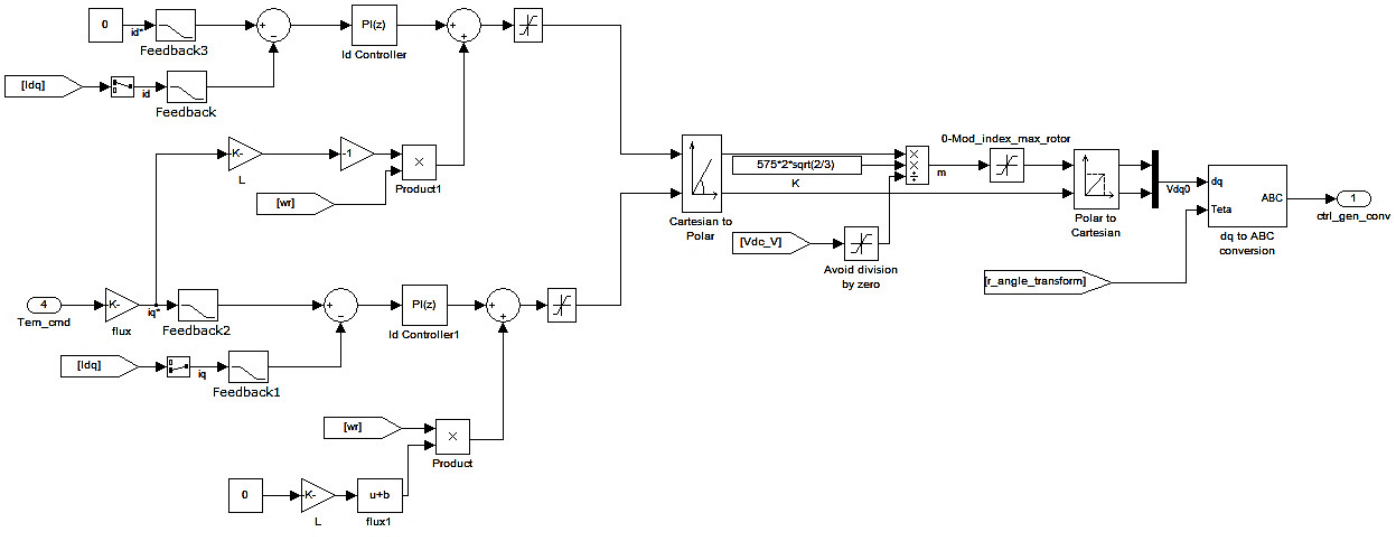

Figure 4.26 Simulink model for the generator-side converter control.

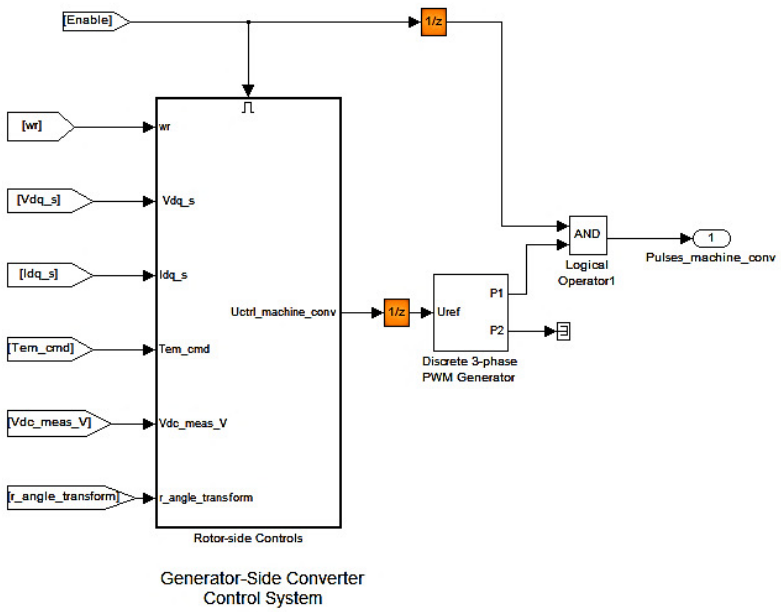

Figure 4.27 Simulink block for the generator-side converter control.

The Discrete PWM Generator block shown in Figure 4.27 is available in the Extras/Discrete Control Blocks library of SimPowerSystems. It generates pulses for carrier-based pulse width modulation (PWM) converters. The block can be used to fire the forced-commuted devices (e.g. field effect transistor (FETs), gate turn-off thyristors (GTOs), or in this case, insulated-gate bipolar transistor (IGBTs)) of 2-level or 3-level converters using a single bridge or two bridges connected in twin configuration. The vectorised outputs P1 and P2 contain either 6 pulses (2-level) or 12 pulses (3-level). The output P1 is used when operating in single-bridge configuration. The modulating signals can be applied at input 1 (Uref). For our system, Here, a 2-level converter with a carrier frequency of 1600Hz has been used.

4.3.3.2 Grid-Side Converter Control

The main function of the control module for the grid-side converter is to stabilize the DC link voltage at its nominal value and also to ensure that the active power generated by the generator is fed to the grid where the capacitor voltage always varies during wind turbine operation. There are many control strategies used for the grid-side converter depending on the reference frame used to perform control strategies. Here, the synchronous reference frame control strategy is investigated. The dynamic model of the grid connection, in the qd reference frame rotating synchronously with the grid voltage, is given as follows [58]:

$$v_{gd} = v_{id} + Ri_{gd} - L\frac{d}{dt}i_{gd} - \omega_g L i_{gq} \tag{4.23}$$

$$v_{gq} = v_{iq} - Ri_{gq} - L\frac{d}{dt}i_{gq} - \omega_g L i_{gd} \tag{4.24}$$

where L and R are the grid inductance and resistance, respectively, and v_{id} and v_{iq} are the inverter voltage components.

Figure 4.28 shows the control diagram for the main grid-side converter implemented in synchronous rotating qd reference frame with its d-axis oriented with the grid voltage vector. The PI regulators with cascade control loops are employed in the grid-side converter control scheme, in which the outer control loops are for DC-link voltage and reactive power regulation, and the inner control loops are for grid side inductor current regulation. To decouple the q-axis and d-axis current control in the grid-side control loop, the feedforward compensation terms are introduced to control the d-axis component for the active current regulation and the q-axis component for the reactive current regulation.

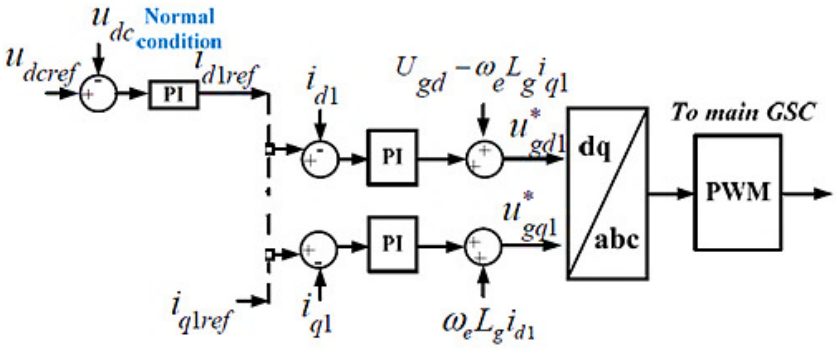

Figure 4.28 Block diagram of the grid-side converter control.

Under normal conditions, dual closed-loop control is applied to the d-axis control, where the outer DC-link voltage loop outputs the reference current for the inner current loop, thereby controlling the DC-link voltage to be constant. This structure ensures that the active power output of the generator may be fed through the converter and into the grid in a timely manner. Single closed-loop control is used for the q-axis control, where the pre-set value of the reactive power determines the reactive current reference. Figure 4.29 depicts the Simulink model for the grid-side control system and Figure 4.30 shows the overall grid-side converter block.

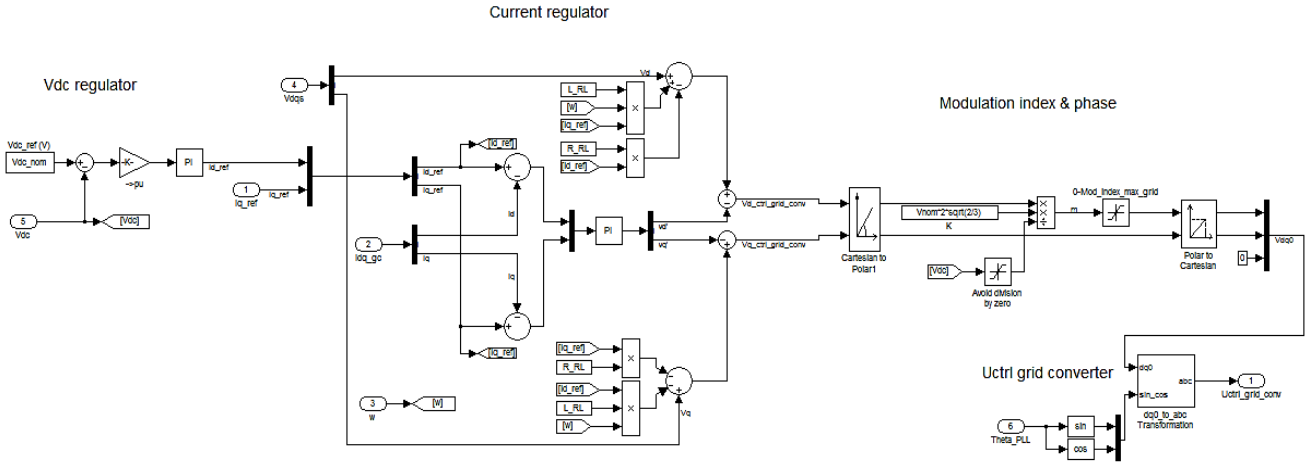

Figure 4.29 Simulink model for the grid-side converter control.

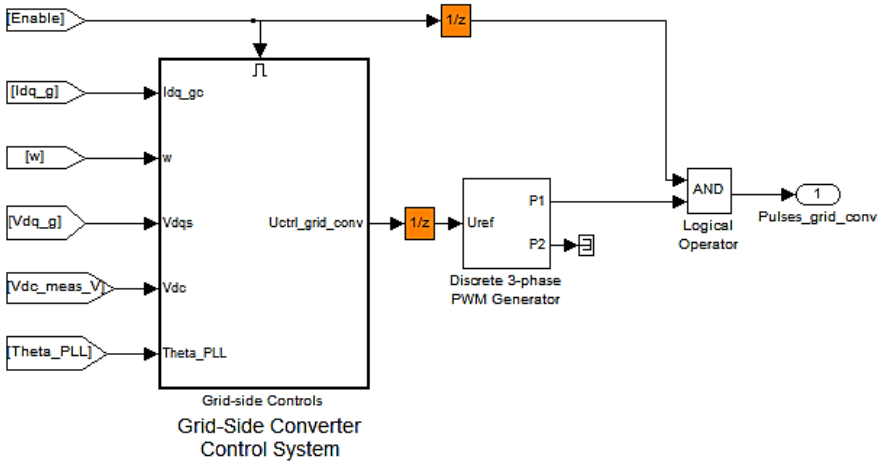

Figure 4.30 Simulink block for the grid-side converter control

The discrete 2-level 3-phase PWM generator depicted in Figure 4.30 is the same one as that used and explained in section 4.3.3.1 with a carrier frequency of 2700Hz.

4.3.4 Wind Turbine Speed Regulator/Torque Control

The target optimum power from a wind turbine can be written as [59]:

$$P_{max} = K_{opt}\omega_{r\_opt}^{3} \tag{4.25}$$

Where,

$$K_{opt} = \frac{0.5\pi\rho c_{p\_max} R^5}{\lambda_{opt}^3} \tag{4.26}$$

$$\omega_{opt} = \frac{\lambda_{opt} v_{wind}}{R} \tag{4.27}$$

During the operation of wind turbine, when the wind speed changes, the generator-side converter controls the q-axis component of the stator current, which regulates the electromagnetic torque of the generator; thus, the turbine rotation speed is adjusted to ensure that operations remain at an optimum tip speed ratio, which corresponds to the maximum power extracted by the wind turbine. In normal conditions, to achieve the MPPT through real-time tracking of the wind turbine maximum wind power curve, the active power reference of PMSG wind turbine is set according to equation 4.28 and represented by Figure 4.31:

$$P_{opt} = K_{opt}\omega_r^3 \tag{4.28}$$

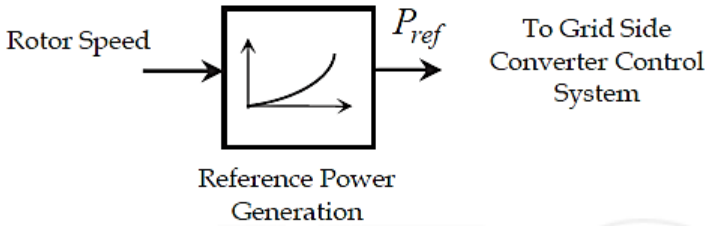

Figure 4.31 Reference power generation for PSF control

The power signal feedback (PSF) control block generates the reference power command P_{ref} using equation 4.28 which is then applied to the grid side converter control system for maximum power extraction. Figure 4.32 depicts the Simulink model for the speed regulator/torque control.

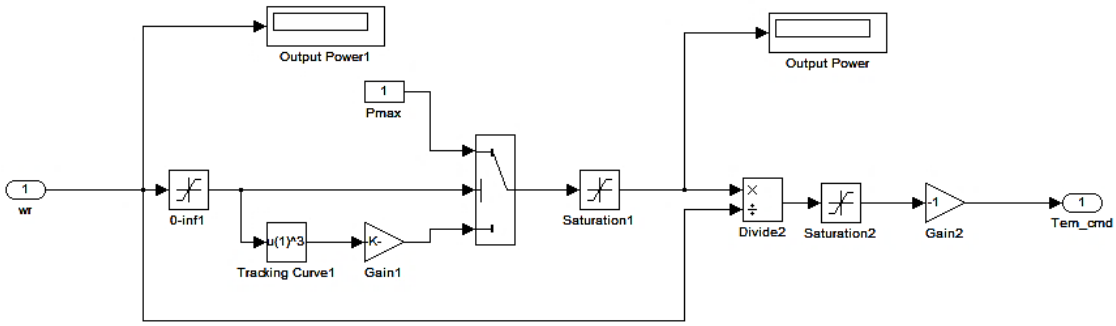

Figure 4.32 Simulink model for wind turbine speed regulator

4.3.5 Simulink Model for the Complete Grid-Connected Wind Turbine Model

Having elaborated the components of the wind turbine system with the necessary equations and figures, the entire system was constructed as depicted in Figure 4.33 and masked into a block in Simulink as shown in Figure 4.34. The entire model was simulated as shown in Figures 4.35-4.39. The system was simulated under nominal conditions (i.e. wind speed = 10 m/s).

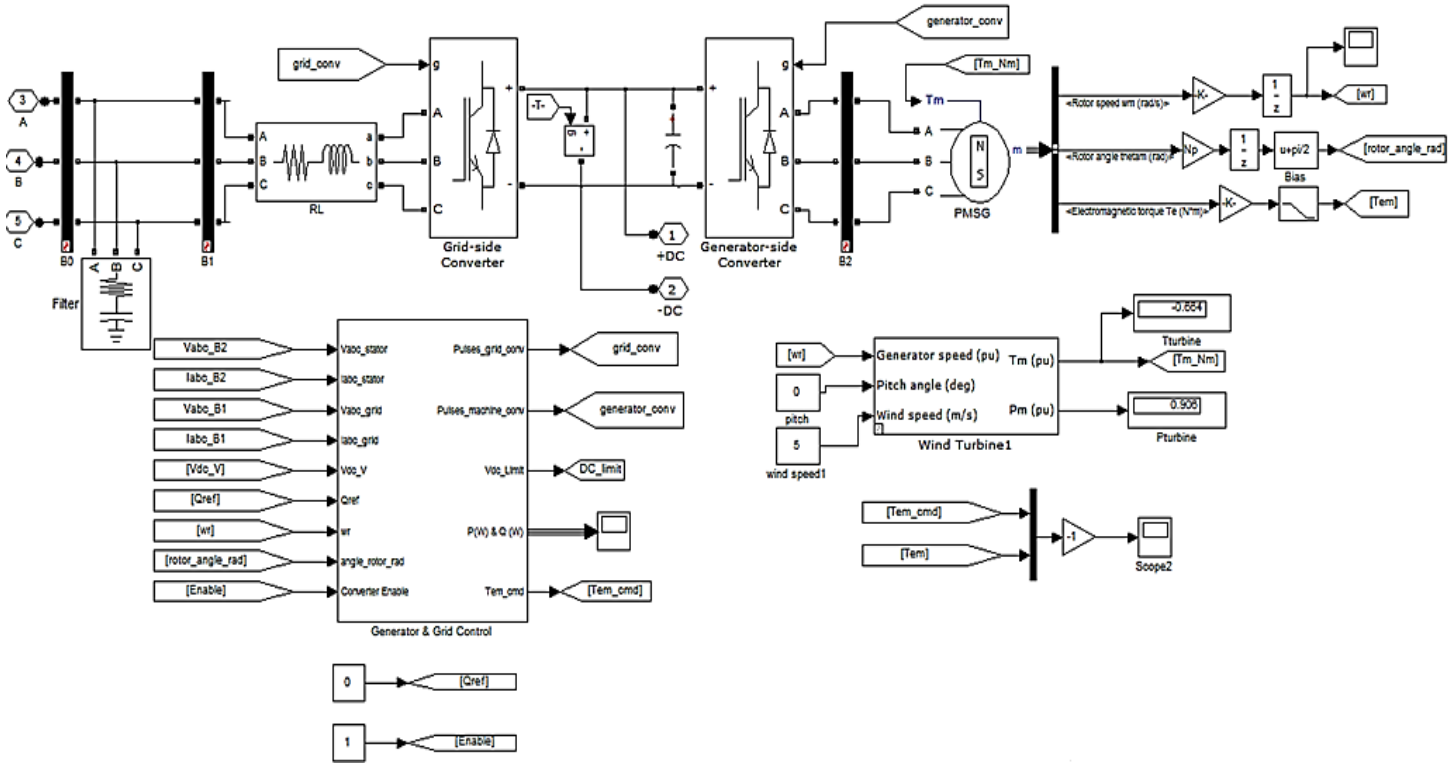

Figure 4.33 Simulink model for the complete grid-connected wind turbine model.

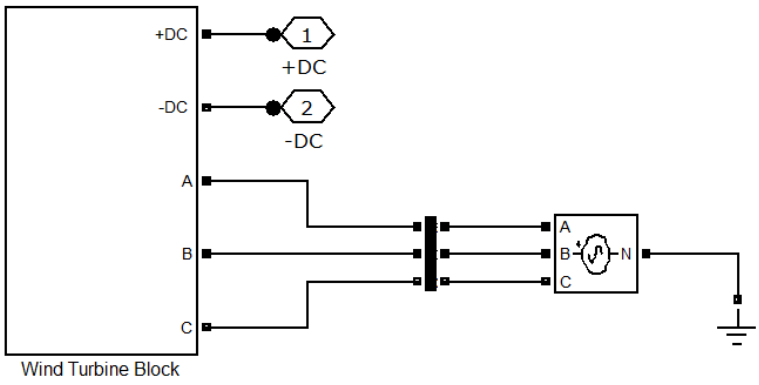

Figure 4.34 Complete wind turbine mask Simulink block.

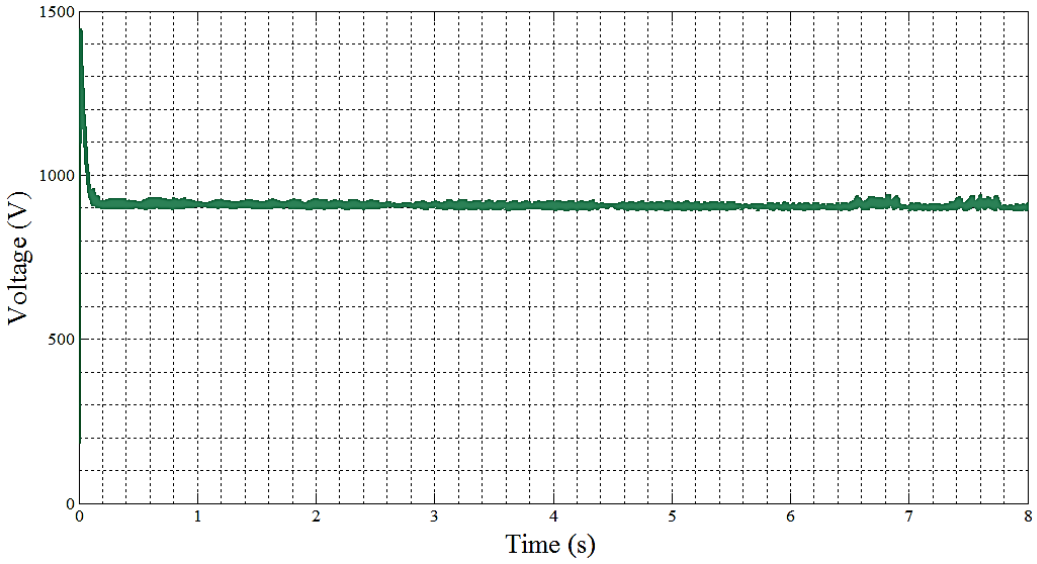

Figure 4.35 Output DC Voltage of the wind turbine DC bus.

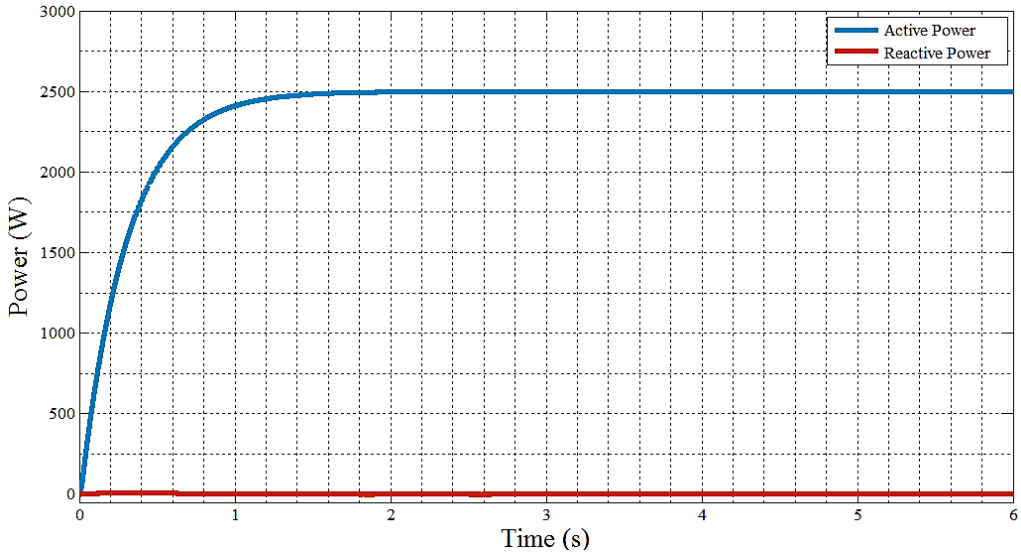

Figure 4.36 Output active and reactive power of the wind turbine system.

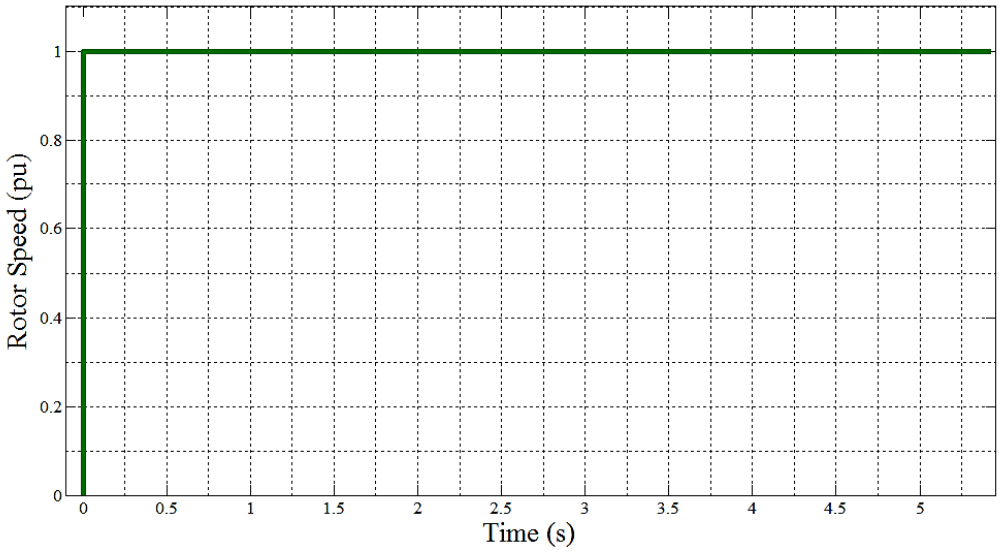

Figure 4.37 Rotor speed (ω_r) of the wind turbine system.

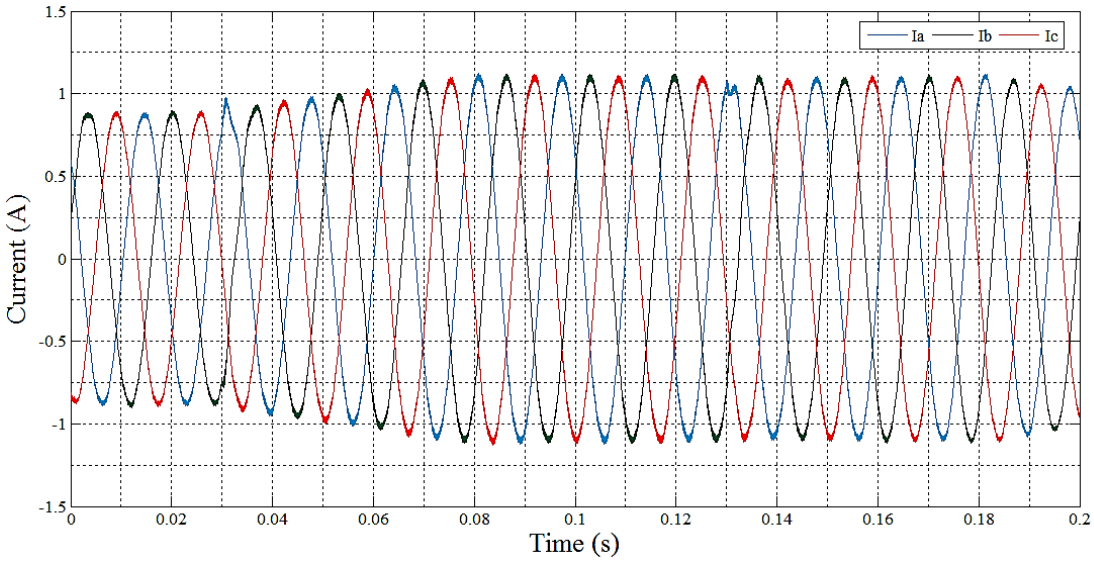

Figure 4.38 Output 3-phase current of the wind turbine system.

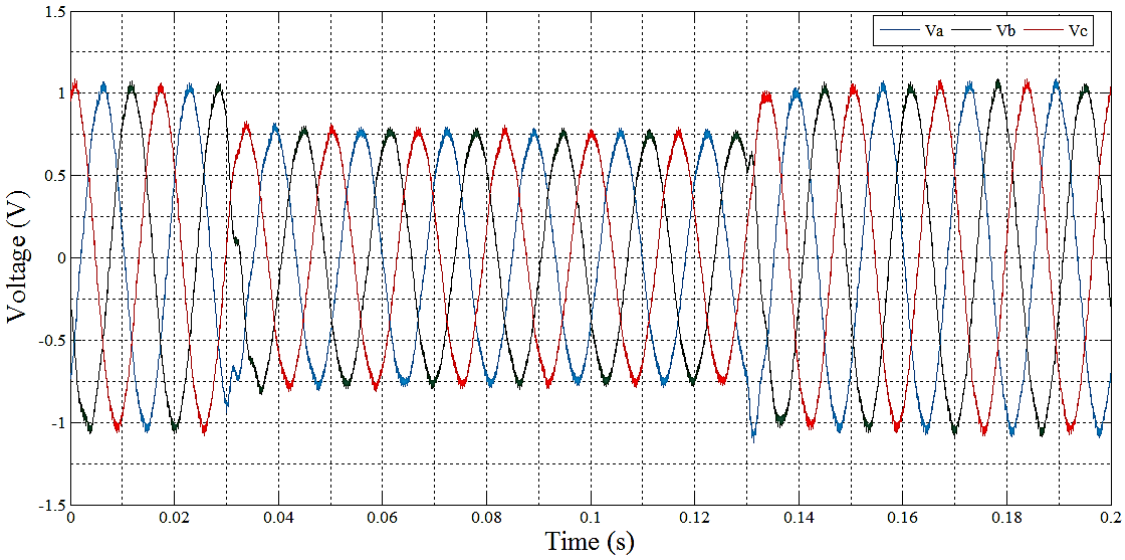

Figure 4.39 Output 3-phase voltage of the wind turbine system.

4.3.6 Wind Turbine Bidirectional Buck-Boost DC-DC Converter

Due to the random characteristics of the wind, the electric power generated by the wind turbine can be of poor quality which fails to meet the normal demand of the load, so an effective reserve or bidirectional energy management system becomes especially necessary. At the working speed of wind, the bidirectional energy management system should convert the wind energy to the stable, reliable electric energy required for the battery charging - in the case of the proposed

system, this is the "buck" mode of the bidirectional DC-DC converter which acts to lower the output voltage of the wind turbine from approximately 915 V down to almost 230 V. When the wind speed decreases significantly and the electric energy generated by the PV is higher than what is required to satisfy the load's demand and the battery is fully charged, the wind turbine bidirectional energy management system sends the excess of energy in the DC bus to the grid – hence, in the case of the proposed system, the bidirectional converter works in "boost" mode to send the energy from the PV to the grid.

A bidirectional buck-boost converter is basically a DC-DC regulator which provides an output voltage that may be less than or greater than the input voltage - hence the name "buck-boost". Among all the topologies that are used to buck as well as boost the voltage, buck-boost converter has wider acceptance as it provides a significant improvement in performance and efficiency by eliminating the transition region between buck and boost modes [60, 61]. The circuit arrangement of the wind turbine buck-boost converter is depicted in Figure 4.40.

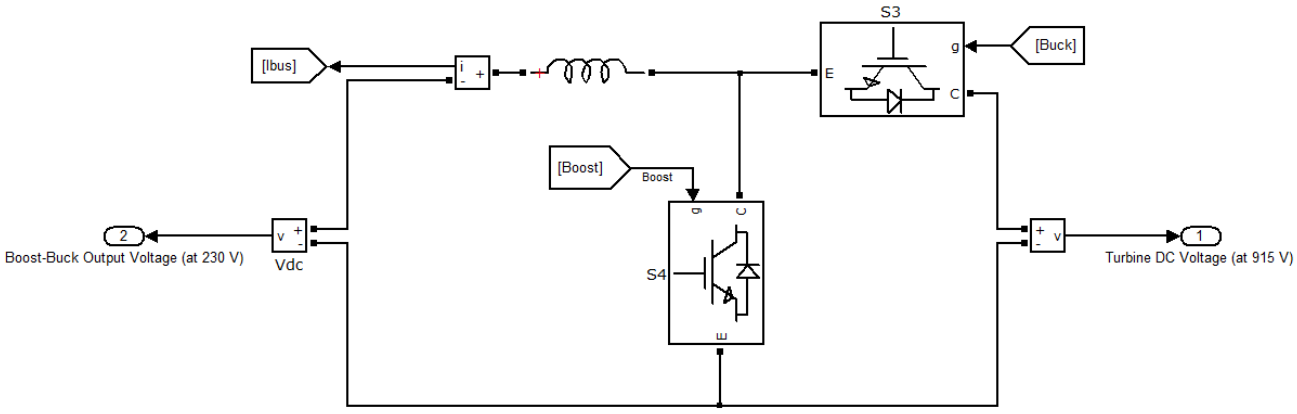

Figure 4.40 Wind turbine bidirectional DC-DC buck-boost converter.

IGBTs or MOSFETs are used as the switching devices in the circuit. The operation of the wind turbine bidirectional converter is controlled by the DC link voltage, V_{dc} and the current of the inductor element, I_{bus}. The main purpose of the bidirectional DC-DC converter is to maintain the voltage of the DC link relatively constant at a reference value. Hence, in view of the instability of the output voltage of the converter, the output voltage requires a voltage stabilising controller. Only in this way can it be used for charging the battery abidingly. The output voltage of the bidirectional converter always relies on the correct detection of the control system which decides

what mode – i.e. buck or boost – the bidirectional converter is in. Figure 4.41 depicts the system designed to control and stabilise the output DC voltage of the bidirectional converter at a constant value of 230 V.

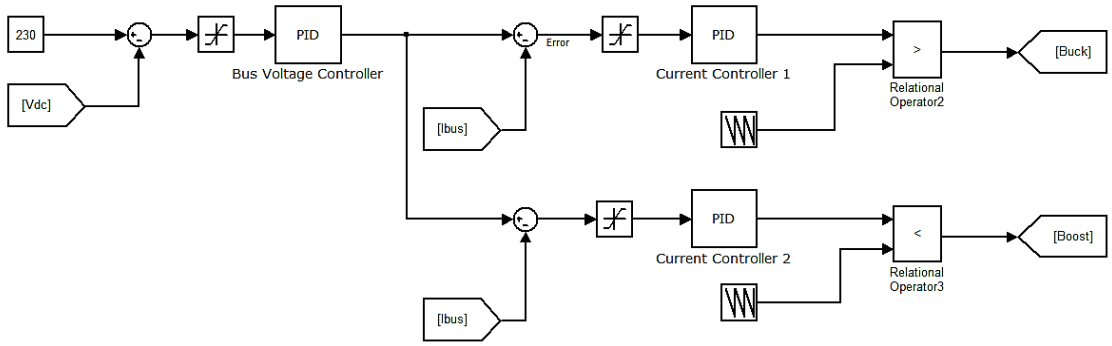

Figure 4.41 Wind turbine bidirectional DC-DC converter controller system.

Under the controlling strategy of the topology depicted in Figure 4.41, the DC-DC converter operating modes can be divided into two main operating modes:

• Mode 1: The bidirectional DC-DC converter acts in buck mode when the DC link voltage V_{dc} (initially 915 V) is greater than the reference value, V_{ref} (230 V). In this mode, the DC-DC converter controls the current to charge the battery.

• Mode 2: The bidirectional DC-DC converter acts in boost mode when the DC link voltage V_{dc} falls below the reference value, V_{ref} (230 V). In this mode, if the energy generated by the PV is higher than what is required to satisfy the load's demand and the battery is fully charged, the PV system sends its energy to the grid.

4.4 Modelling of the Energy Storage System

Batteries are an essential part of the wind-solar generator system and with the acceptance and usage levels increasing, this technology offers a unique and high growth opportunity for battery vendors. Moreover, with a wide range of batteries available that are reliable and cost effective, they offer the best solution to the wind-solar energy storage system to date. They offer an environmentally friendly energy source that is bound to have a greater impact as the years go. Of all rechargeable batteries, Lead-acid batteries have been widely adopted [62].

Lead-acid batteries are the most commonly used type of battery in wind-solar hybrid energy storage systems [62]. Although this type of batteries have a low energy density, only moderate efficiency and high maintenance requirements, they also have a significantly long lifetime and low costs compared to other battery types. One of the singular advantages of Lead-acid batteries is that they are the most commonly used form of battery for most rechargeable battery applications, and therefore have a well-established, mature technology base.

4.4.1 General Notions for Battery

Before the Simulink model for the battery is presented, some fundamental concepts of the battery are briefly reviewed [63]:

1) Nominal Voltage (V): This is the nominal voltage (V_{nom}) of the battery (Volts). The nominal voltage represents the end of the linear zone of the discharge characteristics.

2) Rated Capacity (Ah): This is the rated capacity (Q_{rated}) of the battery in ampere-hour. The rated capacity is the minimum effective capacity of the battery.

3) Initial State-Of-Charge (%): The initial State-Of-Charge (SOC) of the battery. 100% indicates a fully charged battery and 0% indicates an empty battery. This parameter is used as an initial condition for the simulation.

4) Maximum Capacity (Ah): This is the maximum theoretical capacity (Q), when a discontinuity occurs in the battery voltage. This value is generally equal to 105% of the rated capacity.

5) Fully Charged Voltage (V): This is the fully charged voltage (V_{full}), for a given discharge current. It should be noted that the fully charged voltage is not the no-load voltage.

6) Nominal Discharge Current (A): This is the nominal discharge current, for which the discharge curve has been measured. For example, a typical discharge current for a 1.5 Ah NiMH battery is 20% of the rated capacity: ($0.2 * 1.5\,Ah\,/\,1h = 0.3A$).

7) Internal Resistance: This is the internal resistance of the battery (ohms). When a preset model is used, a generic value is loaded, corresponding to 1% of the nominal power

$(nominal\ voltage\ *\ rated\ capacity\ of\ the\ battery)$. The resistance is supposed to be constant during the charge and the discharge cycles and does not vary with the amplitude of the current.

The Simulink battery model is depicted in Figure 4.42:

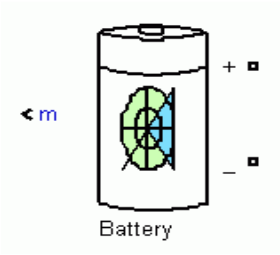

Figure 4.42 Simulink battery block.

The Simulink battery block implements a generic dynamic model parameterized to represent most popular types of rechargeable batteries. The equivalent circuit of the battery is shown in Figure 4.43:

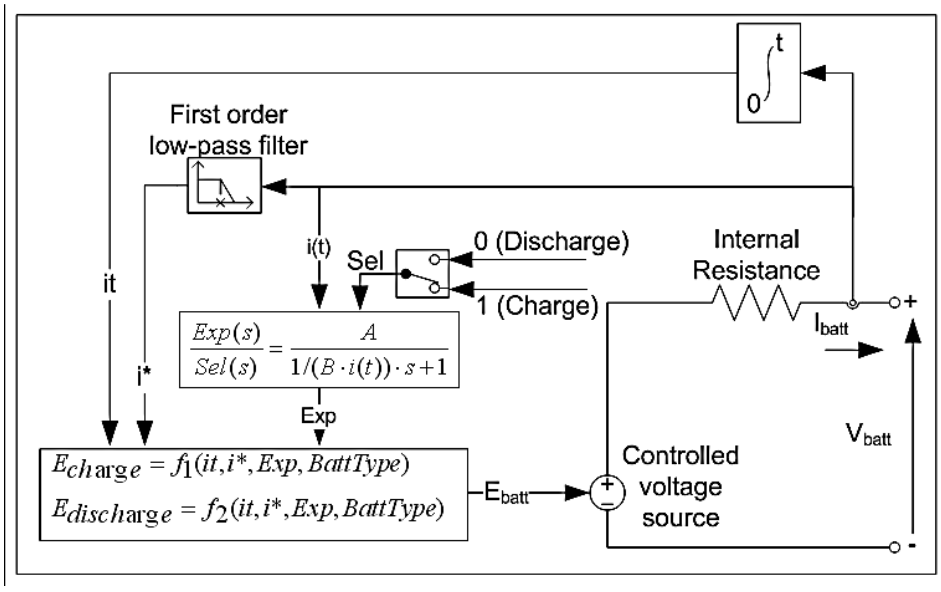

Figure 4.43 Rechargeable battery equivalent circuit.

The Simulink Lead-acid battery model has its particular battery charging and discharging characteristics which can be modelled using the a simple set-up depicted in Figure 4.44:

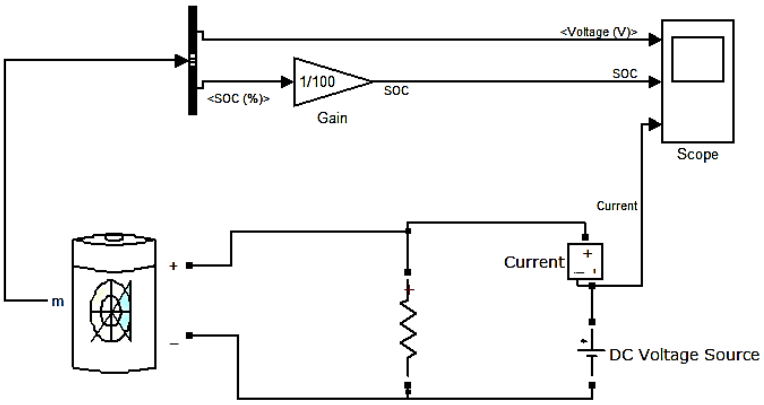

Figure 4.44 Battery charging and discharging characteristics.

In Figure 4.44, the power of the battery is being dissipated through the resistor and simultaneously, it is being charged by a DC voltage source. The value of the battery's SOC varies as the value of the DC voltage changes, so that if the DC voltage is more than the nominal voltage of the battery, then the SOC will remain the same. However, if the DC voltage is less than the nominal voltage of the battery then the SOC will decrease.

4.4.2 Battery Bidirectional DC-DC Converter

The bidirectional DC-DC converter along with energy storage has become a promising option for many power related systems, including hybrid wind-solar systems, electric vehicles, fuel-cell vehicles, and so forth. It not only reduces the cost and improves efficiency, but also improves the performance of the system [63]. In a wind-solar system, the battery bidirectional DC-DC converter is often used to transfer the solar energy to the capacitive (battery) energy source during the times when the wind speed and solar irradiation levels are sufficient, while to deliver energy to the load when the DC bus voltage is low.

A battery buck-boost type high-performance bidirectional converter, as shown in Figure 4.45, is used to charge and discharge the battery. This particular bidirectional converter has the following properties which help enhance its performance [63]:

- Power flow with large voltage diversity
- Soft switching and zero voltage switching
- Reduced switching losses due to fewer switches

• Less conduction losses

• Synchronous rectification

• No transformers

• No magnetizing current saturation

• Less weight and volume

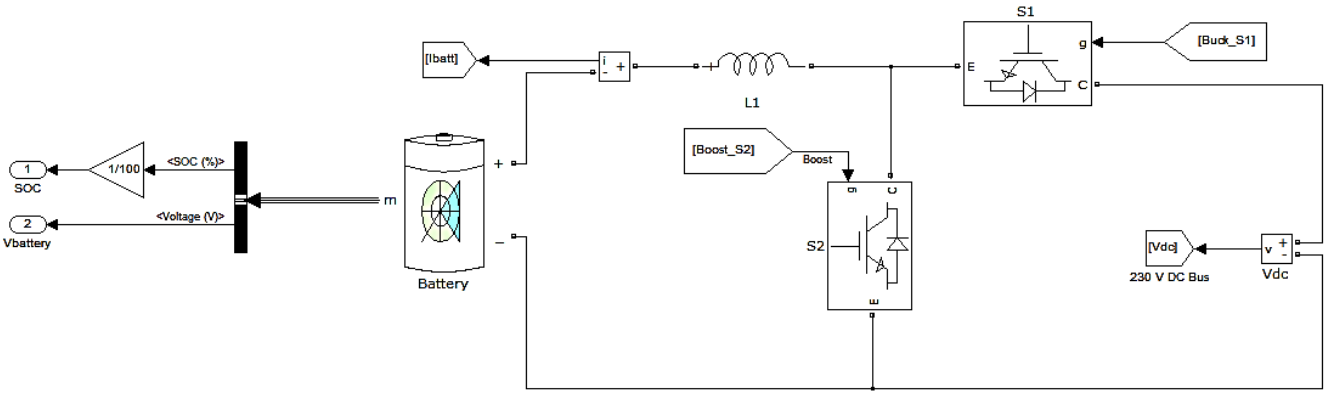

Figure 4.45 Battery Bidirectional DC-DC converter circuit.

As shown in Figure 4.45 the DC-DC (buck-boost) bidirectional converter consists of two main switches (S_1, S_2) with an inductor. S_1 and S_2, once activated, are responsible for maintaining the buck mode and boost mode, respectively. The control topology of the bidirectional DC-DC converter is shown in Figure 4.46.

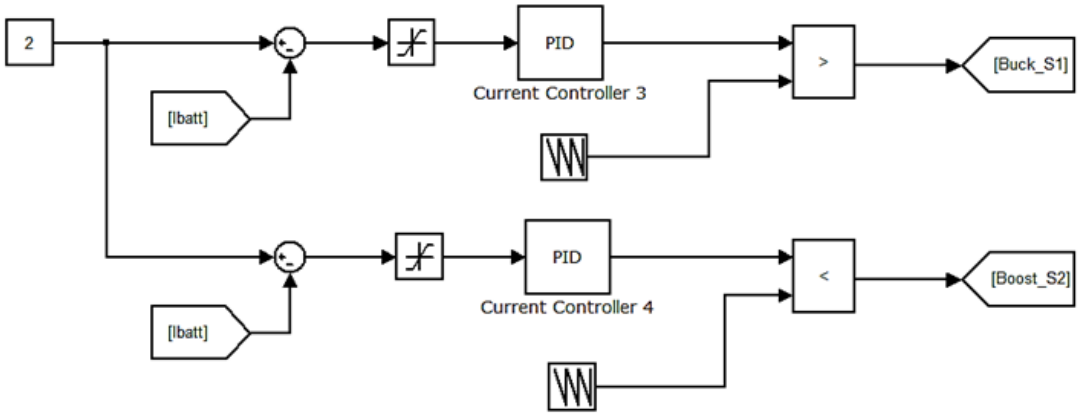

Figure 4.46 Control scheme of the battery DC-DC bidirectional converter.

In the control scheme depicted in Figure 4.46, the battery current, I_{batt} is sensed and compared with the reference current, I_{ref} (which in this case is set to 2 A). The error will be regulated by

the PID current controller. The control signals of buck switch (S_1) and boost switch (S_2) are both generated, where the control law of the boost signal is the complement of the buck signal.

The charging and discharging of the battery during buck and boost mode are depicted in Figures 4.47-4.52. Figures 4.47-4.49 show the status of the current, voltage and the SOC of the battery during buck mode respectively and Figures 4.40-4.52 show the same graphs for the boost mode.

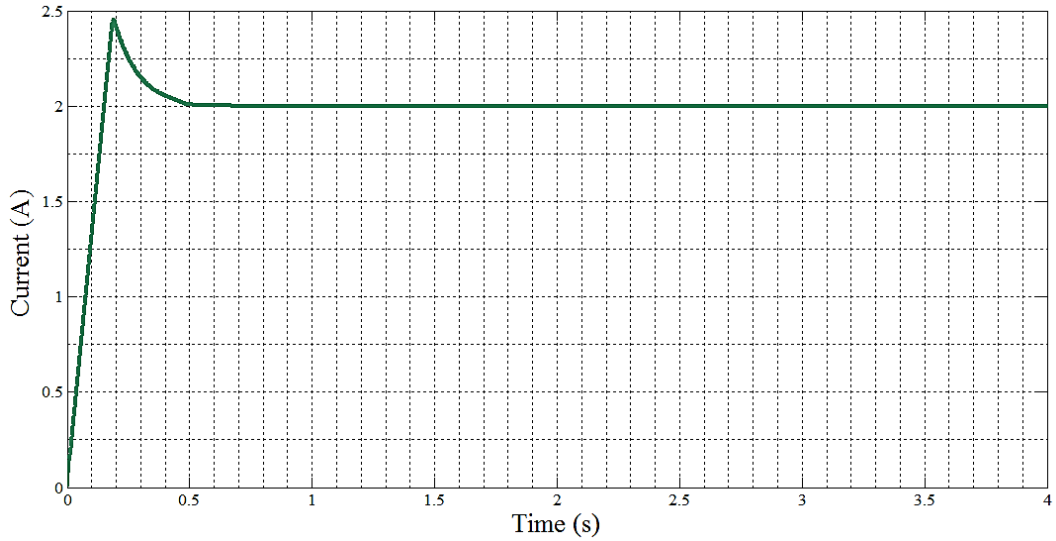

Figure 4.47 Battery's current during buck (charging) mode.

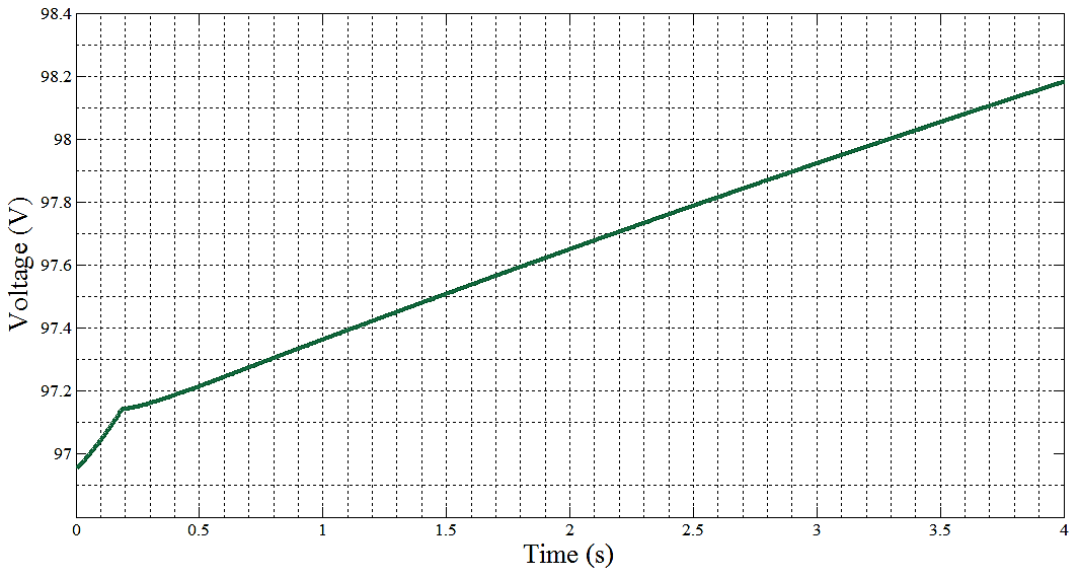

Figure 4.48 Battery's voltage during buck (charging) mode.

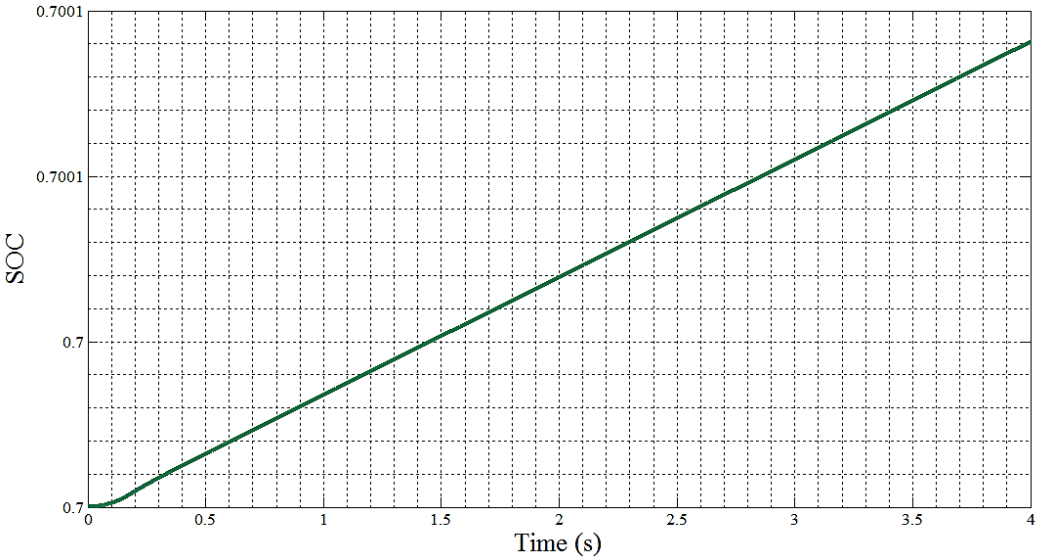

Figure 4.49 Battery's SOC during buck (charging) mode.

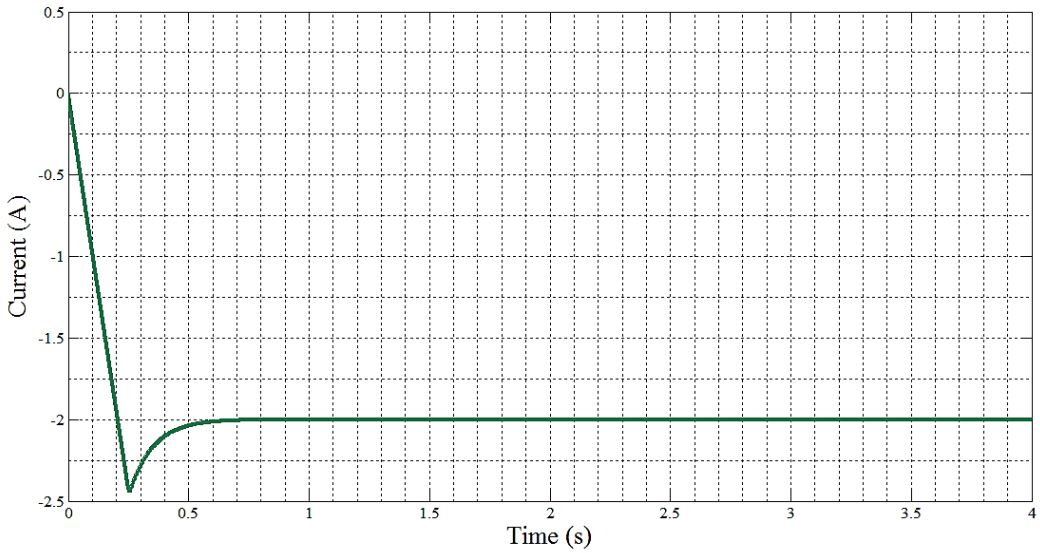

Figure 4.50 Battery's current during boost (discharging) mode.

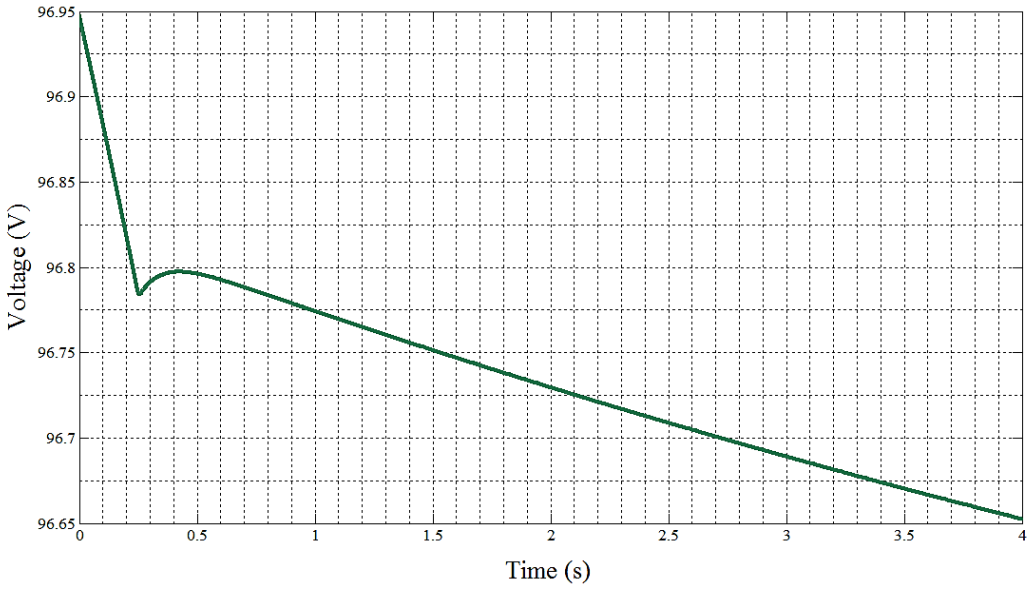

Figure 4.51 Battery's voltage during boost (discharging) mode.

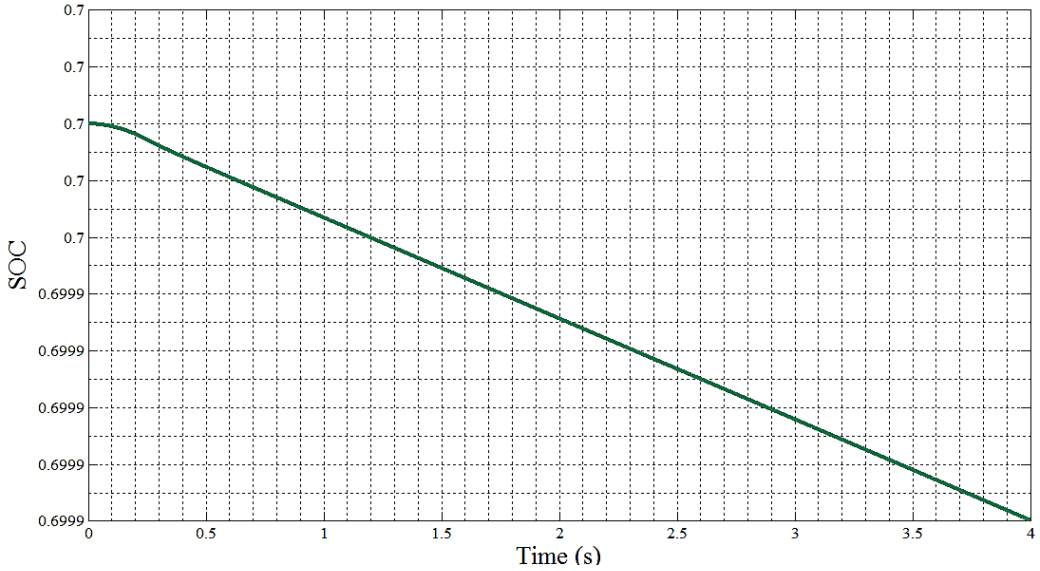

Figure 4.52 Battery's SOC during boost (discharging) mode.

Figure 4.53 shows the connection between the wind-solar system and the battery, where the output DC voltage of the DC link from the wind turbine was fed to the PV and the battery. The entire system was simulated under nominal conditions (namely a solar irradiation of 1 kW/m^2 and a wind speed of 10 m/s) and the results are depicted in Figures 4.54 and 4.55.

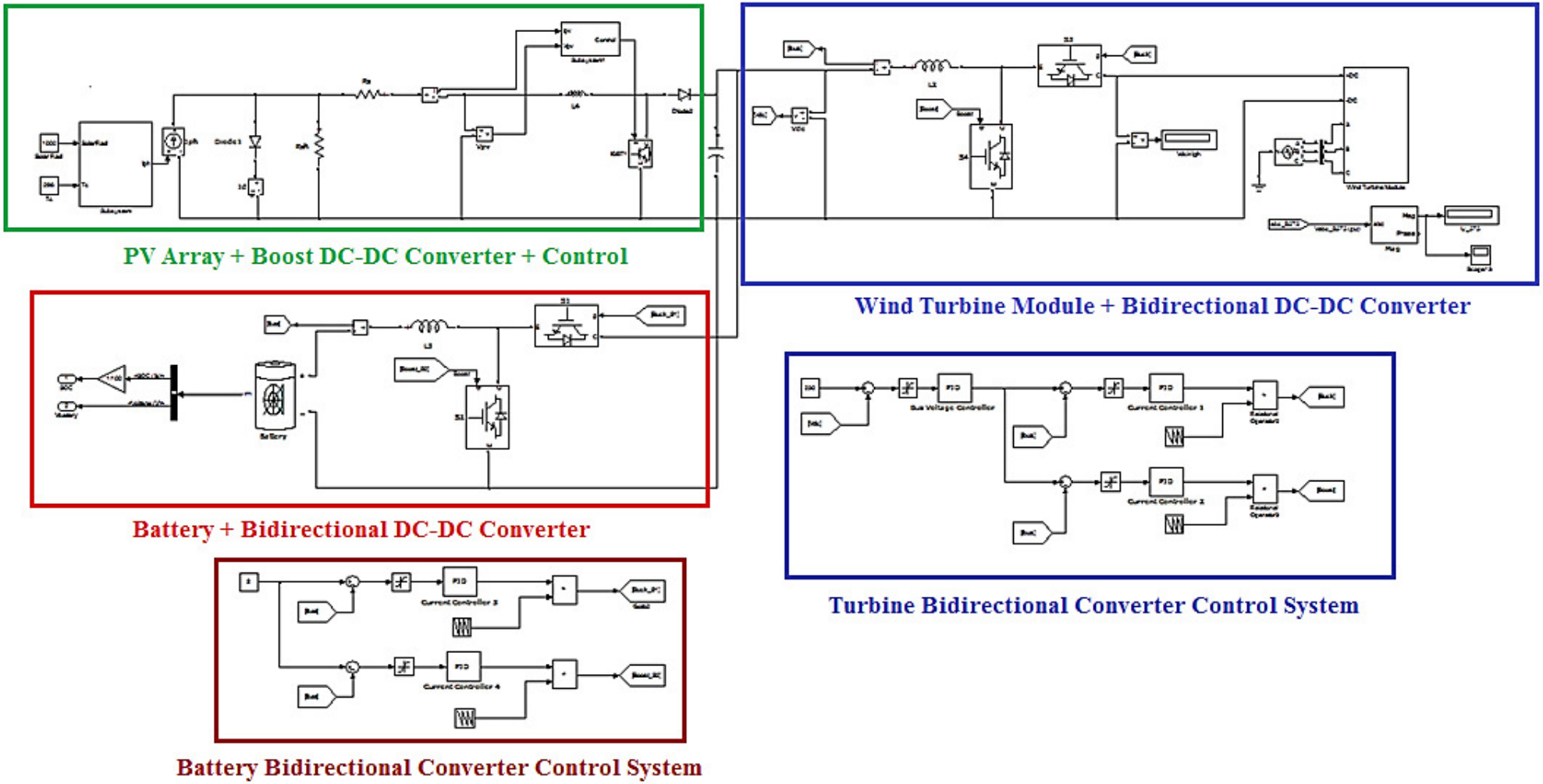

Figure 4.53 Complete wind-solar hybrid system with battery connection.

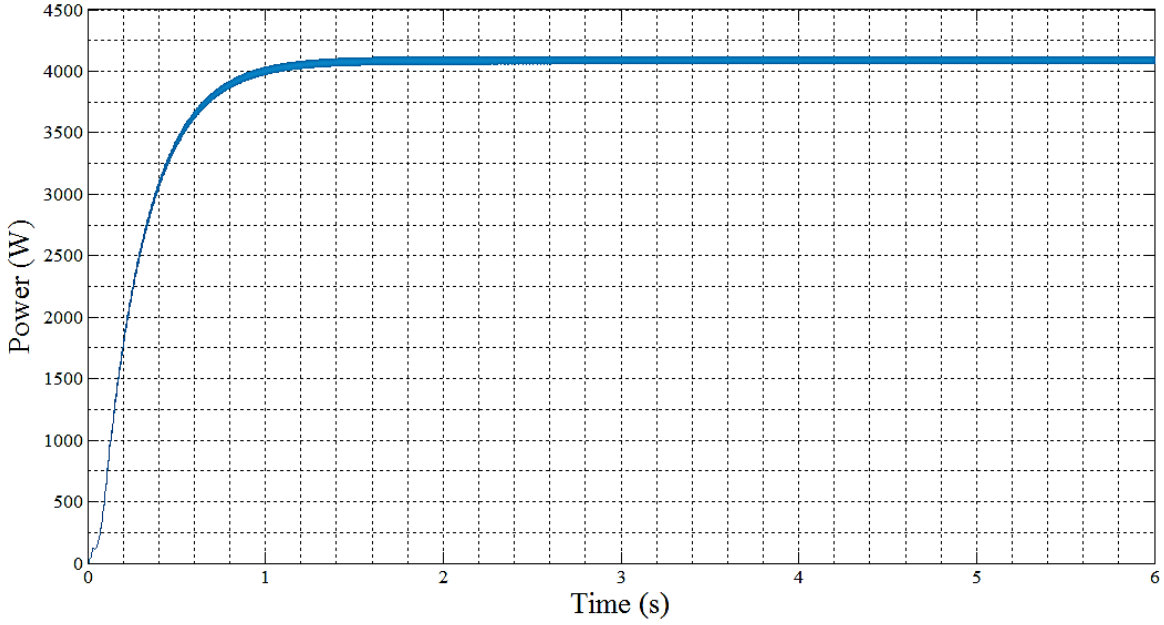

Figure 4.54 Total output power produced by the wind-solar hybrid system.

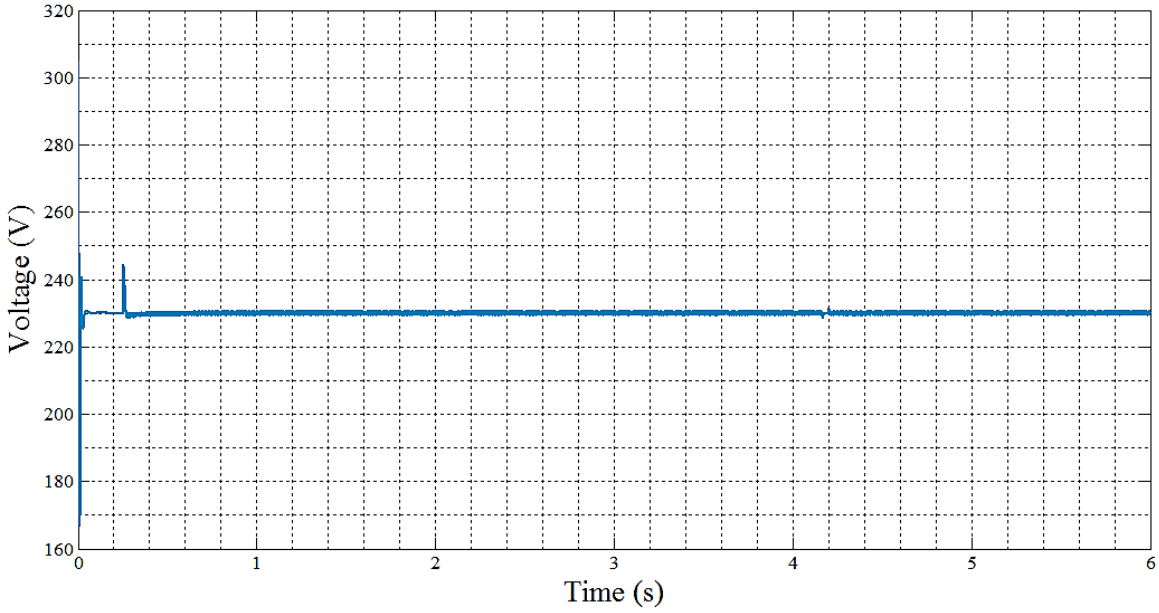

Figure 4.55 Wind-solar hybrid power system DC bus voltage.

5. System Performance and Cost Analysis

5.1 Real-Life System Performance

Monthly average sunshine and daylight hours of Lisbon for the period 2010-2013 were obtained online and depicted in Figure 5.1. Since the average values were very similar throughout the four years, the shown values were assumed to be true for recent times (namely December 2013).

	Jan	Feb	Mar	Apr	May	Jun	Jul	Aug	Sep	Oct	Nov	Dec	Annual
Average Sunlight Hours/ Day	05:11	06:26	06:38	08:50	09:42	11:00	12:11	11:30	09:18	07:27	05:48	05:07	08:16
Average Daylight Hours & Minutes/ Day	09:46	10:41	11:53	13:10	14:15	14:49	14:34	13:38	12:23	11:06	10:01	09:29	12:00
Percentage of Sunny (Cloudy) Daylight Hours	54 (46)	61 (39)	57 (43)	68 (32)	69 (31)	75 (25)	85 (15)	85 (15)	76 (24)	68 (32)	59 (41)	55 (45)	69 (31)

Figure 5.1 Lisbon average sunlight hours per day during each month of the year[3]

In order to simulate and observe the amount of power produced by the proposed PV system, the average monthly solar irradiation was needed, which was obtained from online databases. Figure 5.2 shows the average monthly insolation levels of Lisbon. The position of the solar panel was theoretically adjusted to achieve the highest possible amount of sunshine. As it can be seen in Figure 5.2, solar irradiation is quite high during the summer months (May to August) compared to other months. Since the values for insolation were similar throughout the four years, they were assumed to hold true for 2013 as well. The energy calculations for the proposed PV system installed on a 2-bedroom flat in Lisbon were computed using the number of hours of daylight and the average monthly solar irradiation.

[3] Image obtained online from: http://www.lisbon.climatemps.com/sunlight.php

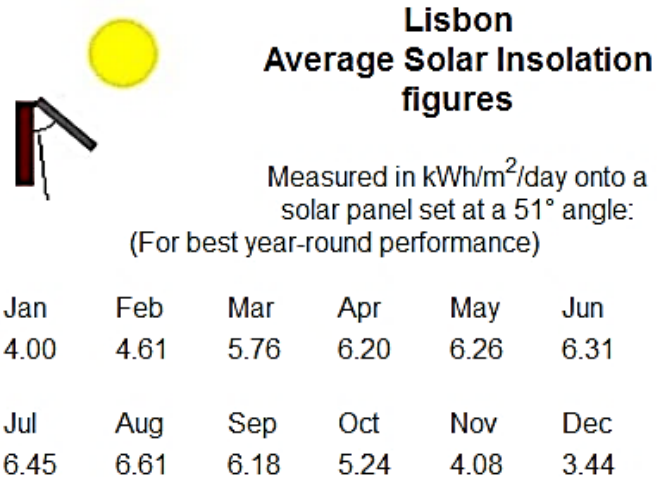

Figure 5.2 Average solar irradiation per day of each month of the year[4]

The hourly energy produced by the PV system was calculated using the following equation:

$$kWh = P_{PV}\ (kW) \times Number\ of\ hours\ of\ daylight\ (h) \tag{5.1}$$

The power produced by the PV system was obtained by simulating the PV system depicted in Figure 4.16 for different average monthly solar irradiation values given in Figure 5.2. Since the insolation values given in Figure 5.2 were in kWh/m^2 and needed to be converted to W/m^2, the following equation was used to obtain the desired values:

$$Solar\ Irradiation\ \left(\frac{W}{m^2}\right) = Solar\ Irradiation\ \left(\frac{kWh}{m^2}\right) \times \frac{1000}{Number\ of hours\ of\ daylight}$$

Afterwards, using equation 5.1, the amount of kWh produced by the PV system was calculated and the results were recorded in Table 5.1.

[4] Data obtained online from: http://solarelectricityhandbook.com/solar-irradiance.html

Table 5.1 Average monthly kWh produced by PV system for different solar radiation values

Month	Average Number Hours of Daylight	Average Monthly Solar Radiation (kWh/m^2)	Average Monthly Solar Radiation (W/m^2)	Average Monthly kWh Produced by PV System
Jan	5.18	4.00	772	5.98
Feb	6.43	4.61	717	6.58
Mar	6.63	5.76	869	7.72
Apr	8.83	6.20	702	8.16
May	9.70	6.26	645	8.20
Jun	11.00	6.31	573	8.20
Jul	12.18	6.45	530	8.36
Aug	11.50	6.61	575	8.54
Sep	9.30	6.18	665	8.14
Oct	7.45	5.24	703	7.18
Nov	5.80	4.08	703	6.02
Dec	5.00	3.44	688	5.42

Next, the monthly average wind speeds in Lisbon for the period 2010-2013 were obtained online[5] as presented in Table 5.2. According to online weather databases, wind speeds are generally higher in the spring season in Lisbon (February to April) compared to other months. This clearly reflects that a wind energy generator system would produce more energy during spring months compared to the other months. The data also shows that there is sometimes a considerable variation of monthly average wind speed of the same month from one year to another. These variations are proof to the fact that the monthly energy output from the wind generator part of the wind-solar hybrid system would be subjected to considerable differences.

[5] Online database is available at: http://www.tutiempo.net/

Table 5.2 Average monthly wind speed for Lisbon, Portugal for 2010-2013

	Average Monthly Wind Speed (m/s)			
Month	**2013**	**2012**	**2011**	**2010**
Jan	2.50	2.72	3.53	3.53
Feb	4.44	3.61	3.28	4.00
Mar	4.72	3.06	3.11	2.97
Apr	4.72	3.25	3.36	3.58
May	5.27	3.39	3.19	3.64
Jun	5.27	3.56	2.38	3.36
Jul	5.55	4.25	4.39	3.64
Aug	5.27	3.50	3.56	3.17
Sep	4.44	3.25	3.19	2.72
Oct	4.44	2.69	3.47	2.89
Nov	3.88	3.17	3.06	3.06
Dec	2.50	2.64	2.90	3.78

Having attained the variations of average monthly wind speeds for Lisbon, the output power produced by the wind generator system during 2013 of Figure 4.33 was obtained and recorded in Table 5.3.

Table 5.3 Average monthly kWh produced by wind turbine for different wind speeds

Month	**Average Monthly Wind Speed (m/s)**	**Average Monthly kW Produced by Wind Turbine**
Jan	2.50	0.12
Feb	4.44	0.26
Mar	4.72	0.35
Apr	4.72	0.32
May	5.27	0.23
Jun	5.27	0.23
Jul	5.55	0.30
Aug	5.27	0.21
Sep	4.44	0.18
Oct	4.44	0.19
Nov	3.88	0.21
Dec	2.50	0.08

For wind turbines which operate based on the variations of wind speed, the total kWh produced was assumed to be the same as the kW of power produced every hour (since, unlike solar irradiation, wind is never non-existent during the day).

Hence, the total amount of kWh produced by the entire wind-solar hybrid system was computed. In order to find out how much this total kWh can contribute towards the total kWh consumption of the 2-bedroom house in Lisbon, average monthly consumption data were obtained by contacting the Energias de Portugal (EDP) services and acquiring the estimated data available for a 2-bedroom residence in a middle-class area of Lisbon. The data were recorded in Table 5.4 and the percentage of energy (kWh) covered by the wind-solar system was calculated.

Table 5.4 Contribution of kWh produced by wind-solar to the daily kWh consumption

Month	Total Average kWh Produced Every Day of the Month by the Wind-Solar System	Wind (kWh)	Solar (kWh)	Total Average kWh Consumed by the Household in Every Day of the Month	Wind-Solar Contribution (%)
Jan	6.1	0.12	5.98	21.4	28.50
Feb	6.84	0.26	6.58	21.2	32.26
Mar	8.07	0.35	7.72	16.32	49.45
Apr	8.48	0.32	8.16	16.6	51.08
May	8.43	0.23	8.2	18.2	46.32
Jun	8.43	0.23	8.2	17.18	49.07
Jul	8.66	0.3	8.36	21.7	39.91
Aug	8.75	0.21	8.54	22	39.77
Sep	8.32	0.18	8.14	18.1	45.97
Oct	7.37	0.19	7.18	15.8	46.65
Nov	6.23	0.21	6.02	19.6	31.79
Dec	5.5	0.08	5.42	22.5	24.44

Figure 5.3 depicts a comparison between the total monthly kWh consumption of the household and the total kWh produced by the wind-solar hybrid system using a column chart.

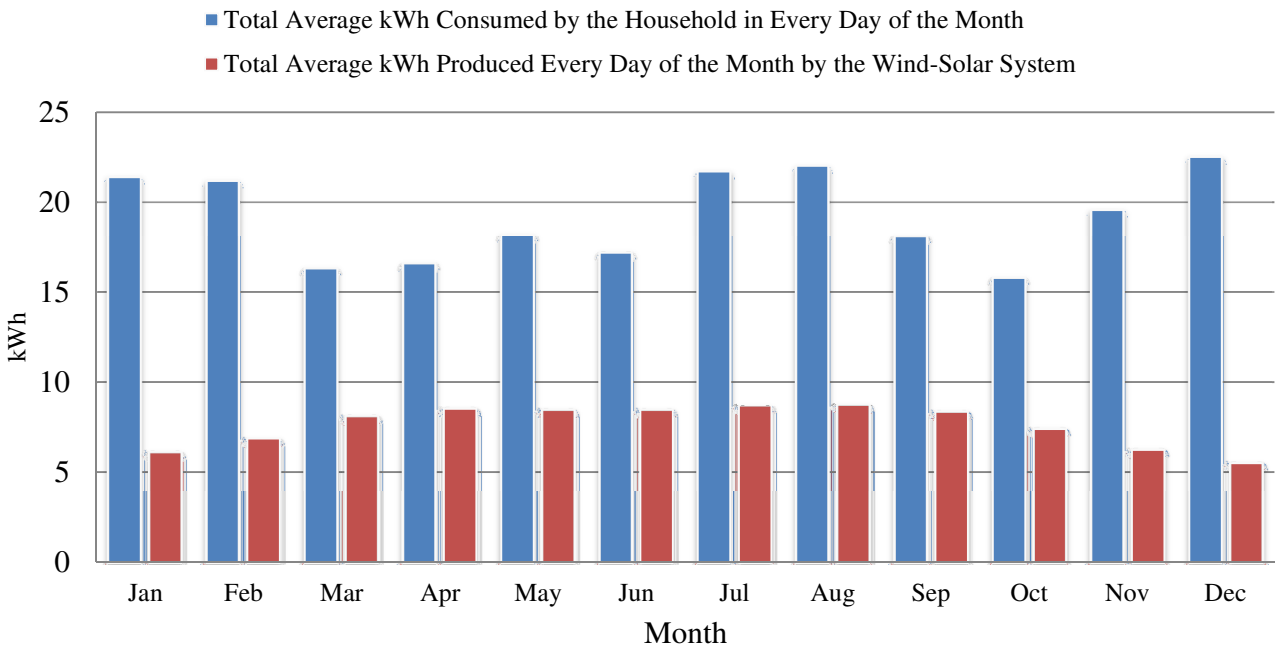

Figure 5.3 Comparison between the total average kWh produced by wind-solar power system and the total average kWh consumed by the household

5.2 Cost Analysis of the Wind-Solar Hybrid System

Before installing the RES, a commonly asked question is "How much does wind-solar electricity cost?" There are practically two questions here, which must be answered separately:

1. What is the upfront cost to install solar? In other words, how much does one have to pay today to have a system installed that delivers a given peak power and a given amount of energy storage?
2. What is the life-cycle cost per kilowatt-hour of solar energy? In other words, how does wind-solar compare to the cost of grid power?

The following approach was used to answer the questions:

1) First, the cost of each major component in terms of user specified variables must be calculated. The major components include: solar panels, wind turbines, inverter, and batteries. The cost of the charge controller will not be added to the rest of the costs here, since this is only a few hundred euros, even that (whereas the whole system cost will be in the thousands of euros). The user specified variables will be: (1) peak power required to power appliances, (2)

total energy produced/consumed per day, (3) hours of sunshine (average), (4) average wind speed.

2) Once the component costs have been calculated, they should be added up to create simple formulas/equations which will be used to answer each of the questions above.

It should be noted that the numbers used below are fairly conservative and include costs such as installation, and so the results should be taken to indicate upper bound estimates. Moreover, simple numbers have been rounded up to simple numbers to make the calculations easier.

5.2.1 Cost of PV Panels as a Function of Energy Usage

The peak power produced by the solar panels is determined by the type and number of solar panels one uses:

$$P_{peak\ panels} = number\ of\ panels \times power\ per\ panel$$

Although the energy used by the appliances will of course be produced by the solar panels, it is not necessary that the peak output of the solar panels be equal the peak power used:

$$P_{peak,usage}: Not\ necessarily\ equal\ to:\ P_{peak\ panels}$$

Instead, it is necessary to calculate the peak power of the solar panels, and hence the number of solar panels, from the total amount of energy required to be produced each day.

Calling the energy produced by the PV system, $E_{produced}$, this value should be equal to the amount of energy used by the PV system each day, so that:

$$E_{produced} = E_{used}$$

The energy is specified in units of kWh using equation 5.1.

The average annual daily target for E_{used} for the proposed PV system is 7.38 kWh (using Table 5.4). Electrical energy from the grid in Portugal costs around 14 cents per kilowatt-hour. In

order to find the electrical costs per day, it is necessary to know the average number of sunlight per day of month, T_{sun}, where:

$$T_{sun} = Average\ hours\ of\ sunshine$$

The average daily value of T_{sun} was found to be 8.25 hours (from Table 5.1). So, for example, if one uses 7.38 kilowatt-hours a day, and the cost of power is about 14 cents per kilowatt-hour, then one's PV electrical costs would be about €1.03 per day, or approximately €31 per month.

Using the formula for power and energy (Power = Energy / Time), it can be written that:

$$P_{peak,panels} = E_{used}/T_{sun} \tag{5.2}$$

As determined from a survey of current market prices, it costs about €1.20/W to purchase and install a PV panel in Europe[6]. Therefore, the upfront cost of the solar panels per kW is $1200/kW$. Thus, as a function of energy use, the cost of the solar panels will be:

$$Cost_{panels} = (E_{used}/T_{sun}) \times €1200/kW$$

Hence, for the proposed PV power generator system, the cost of the PV panels will be approximately:

$$Cost_{panels} = \left(\frac{7.38kWh}{8.25h}\right) \times \frac{€1200}{kW} \approx €1100$$

5.2.2 Cost of Wind Turbine as a Function of Energy Usage

As determined from a survey of current market prices, it costs between about €1000 to €4000 to purchase and install a wind turbine per kW[7]. If it assumed that the cost of a wind turbine is the average of the mentioned numbers, it can be estimated that, $Cost_{WT} = €2500/kW$. Now, if it is estimated that the wind turbine operates with a power of $P_{avg,wind}$ is 1.3 kW (from Table 5.4), it can be concluded that:

[6] Data is available online at: http://www.pv-power-plants.com/industry/national-markets/
[7] Data is available online at: http://www.windenergyfoundation.org/wind-at-work/wind-consumers/wind-power-your-home

$$Cost_{WT} = (P_{avg,wind}) \times Cost_{WT} \quad (5.3)$$

So that $Cost_{WT}$ will approximately be:

$$Cost_{WT} = (1.3kW) \times 2500/kW = €3250$$

5.2.3 Cost of Inverter as Function of Peak Power Required

There are two types of power requirements one needs to know when designing a solar system: The peak power delivered to the load, and the peak power produced by the solar panels by the system. The peak power delivered to the load is the total maximum power level one expects to be drawn by appliances in the home.

The amount of peak power the system can deliver is actually determined by the size of the system's inverter:

$$P_{peak,usage} = P_{peak,inverter}$$

As determined by surveying current market prices for inverters, the costs of an inverter are about €1 per watt, or, $Cost_{inverter} = €100/kW$.

Thus, the cost of the inverter, as a function of the peak power used, is:

$$Cost_{inverter} = P_{peak,usage} \times €100/kW$$

So, for example, if it is assumed that one draws the full 2.5 kW peak power from the inverter systems of the proposed wind system, the cost of the inverter will be approximately $€250$.

5.2.4 Cost of Batteries as a Function of Energy Usage

The amount of energy stored (by batteries) determines how much energy can be used after dark, in particular when there is very little wind. The number of kWh which can be stored will be determined by the number and type of batteries included in the system:

$$E_{stored} = Energy\ per\ battery \times number\ of\ batteries$$

The lifetimes of deep cycle batteries are fairly short (3-10 years), and depend on how well they are maintained (for example, one needs to avoid overcharging, overdrawing, etc.). Presently, the cost of batteries is about €50 per kWh of storage:

$$Cost_{batteries} = €50/kWh$$

The cost of batteries, therefore, *as a function of energy used*, is

$$Cost_{batteries} = E_{used} \times €50/kWh$$

If it is assumed that the Lead-acid battery used in the PV system produces a maximum power of $15\ Ah\ \times 100\ V = 1500\ Wh$ or 1.5 kWh, the cost of the batteries will approximately be:

$$Cost_{batteries} = 1.5\ kWh \times €50/kWh \approx €105$$

5.2.5 Calculation of Upfront Cost

Adding up the costs of the PV panels, wind turbine, inverter, and batteries, it is found that:

$$Cost_{upfront} = Cost_{panels} + Cost_{WT} + Cost_{inverter} + Cost_{batteries}$$
$$\approx €1100 + €3250 + €250 + €75 \approx €4675$$

5.2.6 Payback Period

In order to find out approximately how many years it takes for the investment to return, the total average kWh produced monthly by the hybrid wind-solar power system was calculated using the data from Table 5.4 and was found to be approximately 91.18 kWh. Hence, the average kWh produced daily by the wind-solar system will be equal to $91.18\ kWh\ \div 12 = 7.60\ kWh$. Since electricity is roughly €0.14/kWh in Portugal, the total yearly cost of kWh of the wind-solar system will be $= 7.60\ kWh\ \times €0.14/kWh \approx €1.06$ per day, so that using the system for a year, the consumer will have to pay a total cost of = $€1.06\ \times\ 365\ days \approx €388$.

Since the initial investment cost was found to be €4675 in section 5.2.5, the number of years for which the consumer will have his investment return to him will be:

$$Payback\ Period\ = \frac{€4675}{€388} \approx 12\ years$$

6. Conclusions and Suggestions for Future Work

In this thesis, a new PV-wind turbine hybrid power system was designed, modelled and implemented using the MATLAB/Simulink software package for smart grid applications. As the available power from the proposed PV system is highly dependent on solar radiation, to overcome this deficiency, the PV system was integrated with the wind turbine system. The dynamic behaviour of the proposed model was examined under different operating conditions. Solar irradiance, and wind speed data were gathered for a grid-connected wind-solar power system installed in a residential area in Lisbon. The developed system and its control strategy exhibited an excellent performance. The proposed model offers a proper tool for smart grid performance optimization.

In general, wind-solar hybrid energy systems are recognized as a viable alternative to stand-alone PV or wind systems all over the world. Recent literature reveal that renewable energy based hybrid systems are not cost competitive against conventional fossil fuel power systems. However, the need for cleaner power and improvements in alternative energy technologies bear good potential for widespread use of such systems. Moreover, the less-fortunate rural households in less developed countries attach high value to a reliable, limited supply of electricity.

Although the cost reduction and technological development of hybrid energy systems in recent years has been encouraging, they still remain an expensive source of power. To allow the widespread application of this emerging technology, there is a need for further R&D improvements in solar PV and wind technologies that can reduce the cost of hybrid systems. The cost of conventional energy resources is increasing every year, but the receding trend in the cost of renewable energy technologies because of its widespread use is an encouraging factor, projecting renewable energy systems an economical means of power generation in future for many hybrid and standalone applications. This may finally be concluded that the hybrid energy system combining variable speed wind turbine and PV-array power generating system may be improved by collecting highly accurate hourly data for both solar irradiation and wind speed so that it is possible to estimate the exact continuous power to the load. At the moment, there are no online databases which provide hourly wind speed data for consumers and this itself can be considered as a drawback for one's interest in investing in wind turbine systems. Finally, it is

extremely important to focus on designing the most optimal hybrid controllers in a way to manage the power flow between the system components such that energy cost is minimum and load requirements could be met round the year.

References

[1] IEA (2011), “Energy for All: Financing access for the poor,” OECD/IEA, Oslo.

[2] ARE - shining a Light for a progress, "Hybrid power systems based on renewable energies- A suitable and cost-competitive solution for rural electrification," available at: www.ruralelec.org/fileadmin/DATA/Documents/06_Publications/Position_papers/ARE-WG_Technological_Solutions_-_Brochure_Hybrid_Systems.pdf, Ed.: ARE-Alliance for Rural Electrification, 2008.

[3] Bakos, G., “Feasibility study of a hybrid wind/hydropower system for low-cost electricity production,” in *Applied Energy*, vol. 72. pp. 599-608, Apr 2002.

[4] Karki, R., and R. Billinton, “Reliability/cost implications of PV and wind energy utilization in small isolated power systems,” in *IEEE Transactions on Energy Conversion*, vol. 16, pp. 368–373, 2001.

[5] Elhadidy, M., and S. Shaahid, “Role of hybrid (wind + diesel) power systems in meeting commercial loads,” in *Renewable Energy*, vol. 109-118, Jan. 2004.

[6] Yang, H., Z. Wei, and L. Chengzh, “Optimal design and technoeconomic analysis of a hybrid solar-wind power generation system,” in *Applied Energy*, vol. 86, pp. 163-169, Feb. 2009.

[7] Dihrab, S., and K. Sopian, “Electricity generation of hybrid PV/wind systems in Iraq,” in *Renewable Energy*, vol. 35, pp. 1303-1307, Jun. 2010.

[8] Reichling, J. P., and F.A. Kulacki, “Utility scale hybrid wind-solar thermal electrical generation: a case study for Minnesota,” in *Energy*, vol. 33, pp. 626-638, Apr. 2008.

[9] Ekren O., B. Y. Ekren, and B. Ozerdem, “Break-even analysis and size optimization of a PV/wind hybrid energy conversion system with battery storage – A case study,” in *Applied Energy*, vol. 86, pp. 1043-1054, Jul.-Aug. 2009.

[10] Kim, S. K., J. H. Jeon, C. H. Cho, and E. S. Kim, “Modeling and simulation of a grid-connected PV generation system for electromagnetic transient analysis,” in *Solar Energy*, vol. 83, pp. 664-678, May 2009.

[11] Tsai, H. L., “Insolation-oriented model of photovoltaic module using Matlab/Simulink,” in *Solar Energy*, vol. 84, pp. 1318-1326, July 2010.

[12] Gow, J. A., and C. D. Manning, “Development of a photovoltaic array model for use in power-electronics simulation studies,” in *IEEE Proceedings- Electric Power Applications*, vol. 146, pp. 193-199, Mar. 1999.

[13] Khan, M. J., and M. T. Iqbal, “Dynamic modeling and simulation of a small wind fuel cell hybrid energy system,” in *Renewable Energy*, vol. 30, pp. 421-439, Mar. 2005.

[14] Hossain, M. Zakir, A. K. M. Sadrul Islam, and D.G. Infield, "PV-Wind Hybrid System Modelling for Remote Rural Application," in *Journal of The Institution of Engineers*, vol. 32, pp. 37-44, Dec. 2007.

[15] Chang, J., and Shu-Yun Jia, "Modelling and application of wind-solar energy hybrid power generation system based on multi-agent technology," in *IEEE International Conference on machines learning and cybernetics*, vol. 32, pp. 1754-1758, Jul. 2009.

[16] Castle, John A., James M. Kallis, Sally M. Moite, and Neil A. Marshall, "Analysis of Merits of Hybrid Wind/Photovoltaic Concept for Stand-Alone Systems," in *15th IEEE Photovoltaic Specialists Conference*, vol. 738-744, May 1981.

[17] Technical Brochure No. 145 - CADDET, "A PV-Wind Hybrid System on Bullerö Island, Sweden" available at: www.caddet-re.org/assets/no145.pdf, March 2001.

[18] Nwosu, C. A., and M. U. Agu, "Power and Energy Balance in Wind-Solar Hybrid Power System," in *Pacific Journal of Science and Technology*, vol. 10, pp. 110-116, May 2009.

[19] Femia, N., G. Petrone, G. Spagnuolo and M. Vitelli,, "Optimizing sampling rate of P&O MPPT technique," in *Proceedings of the IEEE 35th Annual Power Electronics Specialists Conference*, pp. 1945-1949, June 2004.

[20] Tariq, A., and M. S. J. Asghar, "Development of microcontroller-based maximum power point tracker for a photovoltaic panel," in *Proceedings of the IEEE Power India Conference, IEEE Xplore*, pp. 5-6, 2006.

[21] Esram, T., and P. L. Chapman, "Comparison of Photovoltaic Array Maximum Power Point Tracking Techniques," in *IEEE Trans, Energy Conversion*, vol. 22, pp. 439-449, 2007.

[22] Menniti, D., A. Burgio, N. Sorrentino, A. Pinnarelli, and G. Brusco, "An incremental conductance method with variable step size for MPPT: Design and implementation," in *Proceedings of the 10th International Conference on Electrical Power Quality and Utilisation*, *IEEE Xplore*, pp. 1-5, 2009.

[23] Xuesong, Z., S. Daichun, M. Youjie and C. Deshu, "The simulation and design for MPPT of PV system Based on Incremental Conductance Method," in *Proceedings of the IEEE WASE International Conference on Information Engineering, IEEE Xplore*, pp. 314-317, 2010.

[24] Dorofte, C., U. Borup, and F. Blaabjerg, "A combined two-method MPPT control scheme for grid-connected photovoltaic systems," in *Proceedings of the European Conference on Power Electronics and Application, IEEE Xplore*, pp. 10-11, 2005.

[25] Mittal, R., K. S. Sandu, and D. K. Jain, "Power Conditioning of Variable Speed Driven PMSG for Wind Energy Conversion Systems", in *2nd WSEAS/IASME International Conference on Renewable Energy Resources*, vol. 8, pp. 189-196, Feb. 2009.

[26] Upadhyay, S. K., Sudhanshu Tripathi, Neeraj Singh, and Gaurav Srivastava, "Optimization and Control of a Variable Speed Wind Turbine with a Permanent Magnet Synchronous

Generator," in *International Journal of Engineering Trends and Technology (IJETT)*, vol. 4, pp. 2620-2627, June 2013.

[27] Sofla, M. A., and Lingfeng Wang, "Control of DC-DC bidirectional converters for interfacing batteries in microgrids," in *Power Systems Conference and Exposition (PSCE), 2011 IEEE/PES*, pp. 1-6, Mar. 2011.

[28] Wei, L. Joos, G., and C. Abbey, "A Parallel Bidirectional DC/DC Converter Topology for Energy Storage Systems in Wind Applications," in *Industry Applications Conference, 2007. 42nd IAS Annual Meeting. Conference Record of the 2007 IEEE*, pp. 179-185, Sep. 2007.

[29] Ramprabhakar, J., and K. Ragavan, "Dual bi-directional converter control for wind-solar-hydro system in grid connected and islanded operation," in *Power Electronics, Drives and Energy Systems (PEDES), 2012 IEEE International Conference*, pp. 1-6, Dec. 2012.

[30] Nema, S., R. K. Nema, and Gayatri Agnihotri, "MATLAB/Simulink based study of photovoltaic cells/modules/array and their experimental verification," in *International journal of Energy and Environment*, vol. 1, pp.487-500, 2010.

[31] Gipe, P. *Wind Power.* London: James & James, 2004.

[32] S. Matthew. *Wind Energy: Fundamentals, Resource Analysis and Economics.* Berlin: Springer, 2006.

[33] American Wind Energy Association, available at: http://www.awea.org/, accessed June September 2013.

[34] Farret, F. A., and M. G. Simões. *Integration of Alternative Sources of Energy*. Wiley-IEEE Press, 2006.

[35] Ibrahimab, H., Adrian Ilincaa, and Jean Perronb, "Comparison and Analysis of Different Energy Storage Techniques Based on their Performance Index," in *IEEE Electrical Power Conference*, pp. 393-398, 2007.

[36] Muljadi, E., and J. T. Bialasiewicz, "Hybrid Power System with a Controlled Energy Storage," in *29th Annual Conference of the IEEE Industrial Electronics Society*, vol. 2, pp. 1296-1301, Nov. 2003.

[37] Linden, D., and T. B. Reddy, *Handbook of batteries*. New York: McGraw-Hill Education, 2002.

[38] Mukund, R. *Wind and Solar Power Systems*. New York: CRC Press LLC, 1999.

[39] Baalbergen, J. F., "System design and power management of a generator-set with energy storage for a 4Q drive," in *Electrical Power Engineering, MSc*: Delft University of Technology, October 2007.

[40] BatteryUniversity.com, "Energy density and Power density, available at: http://www.batteryuniversity.com/partone-5A.htm, Accessed November 2013.

[41] IEEE, "IEEE Recommended Practice for Sizing Lead-Acid Batteries for Photovoltaic (PV) Systems," vol. IEEE Std. 1013-2000, March 2000.

[42] Villalva, M. G., J. R. Gazoli, and E. R. Filho, "Comprehensive approach to modeling and simulation of photovoltaic arrays," in *IEEE Transactions on Power Electronics*, vol. 24, pp. 1198-1208, May 2009.

[43] Modi, B. P., and J. M. Dhimmer, "The temperature dependent ideality factor effect on I–V characteristics of Schottky diode," in *Emerging Technology Trends in Electronics, Communication and Networking (ET2ECN)*, pp. 1-6, Dec. 2012.

[44] Rustemli, S., and F. Dincer, "Modeling of Photovoltaic Panel and Examining Effects of Temperature in Matlab/Simulink," in *Electronics and Electrical Engineering*, vol. 3, pp. 35-40, 2011.

[45] Chander, S., P. Agarwa, and I. Gupta, "Auto-tuned, Discrete PID Controller or DC-DC Converter for fast transient response," in *International Conference on Power Electronics*, pp.1-7, 2011.

[46] Enslin, J. H. R., M. S. Wolf, D. B. Snyman, and W. Sweigers, "Integrated photovoltaic maximum power point tracking converter," in *IEEE Trans. Ind. Electron*, vol. 44, pp. 769-773, 1997.

[47] Pressman, A. I. *Switching and Linear Power Supply, Power Converter Design*. Hayden New Jersey: Hasbrouck Heights, 1977.

[48] Kachhiya, K., Makarand Lokhande, and Mukesh Patel, "MATLAB/Simulink Model of Solar PV Module and MPPT Algorithm," in *Proceedings of the National Conference on Recent Trends in Engineering and Technology*, 2011.

[49] Yadav, A. P. K., S. Thirumaliah, and G. Haritha, "Comparison of MPPT algorithms for dc-dc converters based pv systems," in *International Journal of Advanced Research in Electrical, Electronics, and Instrumentation Engineering*, vol. 1, pp. 18–23, 2012.

[50] Muljadi, E., and C. P. Butterfield, "Pitch-controlled variable-speed wind turbine generation," in *IEEE Trans. Industry Appl.*, vol. 37, pp. 240-246, Feb. 2001.

[51] Lubosny, Z. *Wind Turbine Operation in Electric Power Systems*. Berlin: Springer, 2003.

[52] Heier, Siegfried. *Grid Integration of Wind Energy Conversion Systems*. John Wiley & Sons Ltd, 2006.

[53] Boldea , I. *Synchronous Generators.* United States of America: Taylor and Francis, 2006.

[54] Grenier, D., L. A. Dessaint, O. Akhrif, Y. Bonnassieux, and B. LePioufle, "Experimental Nonlinear Torque Control of a Permanent Magnet Synchronous Motor Using Saliency," in *IEEE Transactions on Industrial Electronics*, vol. 44, pp.680-687, Oct. 1997.

[55] Haque, M. E., M. Negnevistsky, and K. M. Muttaaqi, "A naval control strategy for a variable speed wind turbine with a permanent magnet synchronous generator," in *IEEE Trans Ind Applic*, vol. 26, 2010.

[56] Qiao, W., L. Qu, and R. G. Harely, "Control of IPM synchronous generator for maximum wind power generation considering magnetic saturation," in *IEEE Trans Ind Applic*, vol. 45, 2009.

[57] Chinchilia, M., S. Arnaltes, and J. Burgos, "Control of permanent-magnet generator applied to variable-speed wind-energy systems connected to the grid," *IEEE Trans Energy Convers,* vol. 21, 2006.

[58] Muyeen, S. M., R. Takahashi, T. Murata, and J. Tamura, "A variable speed wind turbine control strategy to meet wind farm grid code requirements," in *IEEE Trans Power Systems*, vol. 25, 2010.

[59] Li, S., T. A. Haskew, and L. Xu, "Conventional and novel control designs for direct driven PMSG wind turbines," in Electrical Power Systems, vol. 80, pp. 328-38, Oct. 2009.

[60] Mitchell, D. M. *DC-DC Switching Regulator Analysis*. New York: McGraw-Hill, 1988.

[61] Mohan, N., T. Undeland, and W. Robbins. *Power Electronics: Converters, Applications and Design*. New York: John Wiley and Sons, 1995.

[62] Duarte, J. L., M. Hendrix, and M. G. Simoes, "Three-port bidirectional converter for hybrid fuel cell systems," in *IEEE Trans. Power Electron.,* pp. 480-487, Mar. 2007.

[63] Wai, R. J., and R. Y. Duan, "High-efficiency bidirectional converter for power sources with great voltage diversity," in *IEEE Trans. Power Electron.*, vol. 22, pp. 1986-1996, Sep. 2007.